DESIGN OF COMPOSITE LAMINATES FOR OPTIMUM FREQUENCY RESPONSE

by

Rengin Kayıkçı

B.S., Mechanical Engineering, İstanbul Technical University, 2005

Submitted to the Institute for Graduate Studies in
Science and Engineering in partial fulfillment of
the requirements for the degree of
Master of Science

Graduate Program in Mechanical Engineering
Boğaziçi University

2008

DESIGN OF COMPOSİTE LAMINATES FOR OPTIMUM FREQUENCY RESPONSE

APPROVED BY:

Assoc. Prof. Fazıl Önder SÖNMEZ ……
(Thesis Supervisor)

Asst. Prof. Bülent EKİCİ ……

Asst. Prof. Çetin YILMAZ ……

DATE OF APPROVAL ……13/06/2008……

ACKNOWLEDGEMENTS

I would like to thank to my thesis supervisor, Dr. Fazıl Önder Sönmez for his guidance and continued support throughout this study.

This study was supported by TUBITAK with the code number 106M301.

ABSTRACT

DESIGN OF COMPOSITE LAMINATES FOR OPTIMUM FREQUENCY RESPONSE

In this study, natural frequency response of symmetric laminated composite plates was optimized. An analytical model accounting for bending-twisting effects was used to determine the laminate natural frequency. In this way, no limitations needed to be imposed on the stacking sequence of laminates to avoid error as in some of the previous studies. Two types of problem, fundamental frequency maximization and frequency separation maximization, were considered. Because of the existence of numerous local optimums, a global search algorithm, direct simulated annealing, was utilized as to find the optimal designs. Results were obtained for different plate aspect ratios. Effects of the number of design variables and the range of values they take on the optimal frequency were also investigated.

ÖZET

TABAKALI KOMPOZİTLERİN OPTİMUM FREKANS CEVABI İÇİN TASARIMI

Bu çalışmada, tabakalı simetrik kompozit plakaların doğal frekans cevabı optimize edilmiştir. Tabakalı plakanın doğal frekans hesaplamasında eğilme-burulma etkilerini hesaba katan analitik bir yöntem kullanılmıştır. Böylece daha önceki bazı çalışmalarda olduğu gibi hatayı engellemek için kısıtlanan tabakalı plakanın fiber yönlerine bu çalışmada herhangi bir kısıtlama getirilmemiştir. Temel frekans maksimizasyonu ve frekans ayırımı maksimizasyonu olmak üzere iki çeşit problem göz önüne alınmıştır. Lokal optimum sayısının çok olmasından dolayı optimal tasarımları bulmak için evrensel bir optimizasyon yöntemi olan direk tavlama simülasyonu kullanılmıştır. Sonuçlar değişik en/boy oranları için bulunmuştur. Tasarım değişkenlerinin sayısı ve alabilecekleri değerler değiştirildiğinde optimal frekansa olan etkileri incelenmiştir.

TABLE OF CONTENTS

ACKNOWLEDGEMENTS iii
ABSTRACT iv
ÖZET v
LIST OF FIGURES vii
LIST OF TABLES viii
LIST OF SYMBOLS / ABBREVIATIONS x
1. INTRODUCTION 1
2. PROBLEM STATEMENT. 6
3. ANALYSIS OF LAMINATED PLATES 8
4. NATURAL FREQUENCY ANALYSIS OF LAMINATED PLATES 12
4.1. Testing the Convergence of the Method 13
4.2. Comparison of the Frequency Analysis Results 16
5. OPTIMIZATION METHOD 18
5.1. Application of DSA Algorithm to the Frequency Optimization Problem . . . 19
6. RESULTS 23
6.1 Comparison of the Optimization Results for Fundamental Frequency Maximization 23
6.2. Comparison of the Optimization Results for Frequency Separation 24
6.3. Results for Different Design Domains 30
6.4. Results for Fundamental Frequency Maximization and Frequency Separation Maximization 33
7. CONCLUSIONS AND FUTURE RESEARCH 40
APPENDIX A: ANALYSIS OF LAMINATED PLATES UNDER SMALL DEFLECTIONS 42
APPENDIX B: BOUNDARY - CONTINOUS FOURIER SERIES FOR THE SOLUTION OF NATURAL FREQUENCY PROBLEM IN LAMINATED RECTANGULAR PLATES 49
REFERENCES 66
REFERENCES NOT CITED 70

LIST OF FIGURES

Figure 2.1. A rectangular laminated plated consisting of multiple lamina 6

Figure 4.1. Convergence of the frequency parameter of the laminate 15

Figure 4.2. Convergence of the vibration response of the laminate 15

Figure A.1. Stress resultants acting on the laminate 44

LIST OF TABLES

Table 4.1. Material properties for graphite-epoxy [10, 28, 29] 14

Table 4.2. Comparison of the frequency parameter values 16

Table 6.1. Material properties for graphite-epoxy [3-5] 23

Table 6.2. Comparison of the optimum angles obtained in this study and previously for frequency maximization 24

Table 6.3. Material properties for T300/5280 graphite-epoxy [7] 25

Table 6.4. Material properties for Scotchply 1002 glass-epoxy [7] 25

Table 6.5. Optimum angles for frequency separation $\Delta\Omega_{12}$ for graphite-epoxy . 26

Table 6.6. Optimum angles for frequency separation $\Delta\Omega_{23}$ for graphite-epoxy . 27

Table 6.7. Optimum angles for frequency separation $\Delta\Omega_{12}$ for glass-epoxy . . . 28

Table 6.8. Optimum angles for frequency separation $\Delta\Omega_{23}$ for glass-epoxy . . . 29

Table 6.9. Optimum angles of frequency separation problem for different discrete angle increments having $[\alpha_4 / \beta_4]_s$ configuration 31

Table 6.10. Optimum angles of frequency separation problem for different discrete angle increments having $[\alpha_2 / \beta_2 / \gamma_2 / \theta_2]_s$ configuration . . 32

Table 6.11. Optimum angles of frequency separation problem for different discrete angle increments having $[\alpha/\beta/\gamma/\theta/\xi/\tau/\varphi/\psi]_s$ configuration 33

Table 6.12. Optimum angles for 8 ply laminate with different aspect ratios for 15° discrete angle increment 35

Table 6.13. Optimum angles for 8 ply laminate with different aspect ratios for 5° discrete angle increment 36

Table 6.14. Optimum angles for 8 ply laminate with different aspect ratios for 1° discrete angle increment 37

Table 6.15. Optimum angles for first and second mode frequency separation for 8 ply laminate with different aspect ratios 38

Table 6.16. Optimum angles for second and third mode frequency separation for 8 ply laminate with different aspect ratios 39

LIST OF SYMBOLS / ABBREVIATIONS

A_{ij}	Laminate extensional stiffnesses
A_t	Acceptability
B_{ij}	Laminate coupling stiffnesses
D_{ij}	Laminate bending stiffnesses
D_0	Reference bending stiffness
E_1	Young's modulus in longitudinal direction
L_k	Length of the kth Markov chain
L_k'	Number of trials executed in the kth Markov chain
M_x, M_y, M_{xy}	Moment resultants per unit width
N	Number of configurations
N_x, N_y, N_{xy}	In-plane force resultants per unit width
P_r	Randomly generated number
Q_x, Q_y	Shear force resultants per unit width
$(\overline{Q}_{ij})_k$	Transformed reduced stiffnesses for the kth layer
T_k	Temperature parameter in the kth Markov chain
V_{rs}, Y_{rs}, Z_{rs}	Plate Fourier coefficients
a , b	Length and width of the rectangular plate
$a_s, b_s, c_r, d_r, \overline{a}_s, \overline{b}_s, \overline{c}_r, \overline{d}_r$	Boundary Fourier coefficients
f_h	Highest cost of the of configurations
f_l	Lowest cost of the of configurations
f_t	Cost of the trial point
h	Height of the laminate
i	Imaginary unit
m, n, r, s	Number of terms in Fourier series
n	Dimension of the optimization problem
(r,s)	Eigenmodes
q(x,y)	Distributed transverse load acting on the plate
q	Dynamic inertia force
t	Time

w(x,y,t), V(x,y)	Assumed solution function for free vibration motion of the laminate
x,y,z	Cartesian coordinate axes
x_d	Jump discontinuity points in d number
ε	Tolerance
$\varepsilon_x, \varepsilon_y, \gamma_{xy}$	Normal and shear strains
$\varepsilon_x^\circ, \varepsilon_y^\circ, \gamma_{xy}^\circ$	Middle-surface strains
θ_k	Current angle of the kth layer
θ_k'	Newly generated angle of the kth layer
$\Delta\theta_{max}$	Maximum angle variation
$\kappa_x, \kappa_x, \kappa_{xy}$	Plate curvatures
ν	Poisson's ratio
$\overline{\rho}$	Mass density of the laminate per unit area
ρ_0	Mass density of the laminate per unit volume
$\sigma_x, \sigma_y, \tau_{xy}$	Normal and shear stresses
Ω_i	Non-dimensional frequency parameter
Ω_1	Fundamental frequency parameter
Ω_2	Second lowest frequency parameter
Ω_3	Third lowest frequency parameter
$\Delta\Omega_{ij}$	Frequency parameter difference between ith and jth frequency parameter
ω	Angular frequency in radian per second
DSA	Direct simulated annealing
SA	Simulated annealing

1. INTRODUCTION

Laminated composite plates are increasingly being used in many different fields such as aerospace, automotive, marine and civil applications. They are attractive for designers because they have superior mechanical properties like high strength-to-weight and stiffness-to-weight ratios, corrosion resistance. Moreover their material system can be changed in many ways such as fiber angles, stacking sequence, composition to obtain desired properties.

In the design of laminated plates, many aspects of their structural behavior should be considered. Especially in structures like aircrafts and spacecrafts where thin plates are used, vibration problems become more important. Fundamental frequency becomes lower with decreased thickness. Considering that continuous fiber reinforced plates are usually desired for applications requiring high specific strength and thus they are required to be thin, they are liable to fail due to resonance under external excitation. Choosing a large thickness far beyond the requirements of strength is against the requirements of light weight and cost effective design. By optimally designing the material system such as fiber orientations, stacking sequence and type and composition of material, one may optimize the natural frequency to avoid resonance without any need to increase thickness.

Forcing frequency often falls in an interval between zero and the fundamental natural frequency, so by maximizing the natural frequency, the range of operating frequency can be increased or the likelihood of resonance can be decreased. There are a number of studies on optimal vibration behavior of laminates. Bert [1] presented results for the maximum fundamental frequency of a simply supported symmetric balanced laminate with a lay-up of $[\pm\theta]_s$. Bert [2] considered the same problem for clamped plates. In both of these studies, bending-twisting effects were approximated with the help of previously known frequencies to obtain a closed-form solution, so a priori knowledge about the fundamental frequency of laminates having certain stacking sequences was needed. Reiss and Ramachandran [3] tried to obtain the optimum design for the same configuration used by Bert [1] using a closed form solution for the frequency of the laminate. Mateus et al. [4] studied the optimal design of thin laminated plates and obtained results for maximum fundamental frequency

and minimum elastic strain energy using finite element method to determine the frequency response. Soares et al. [5] presented a two-level approach for maximizing the natural frequency and minimizing the volume of a plate or shell structure. Both of these studies [4-5] used the same laminate configuration as the one used by Bert [1]. Rao and Singh [6] found minimum weight of a plate subjected to a lower bound constraint on fundamental frequency where the individual lamina thicknesses were design variables.

If the frequency of the external excitation is large, the structure may be designed so that the external frequency is between two adjacent higher order natural frequencies. Maximizing the interval between these frequencies reduces the risk of resonance. Some researchers [7-9] considered the problem of maximum frequency separation. Adali and Verijenko [7] determined the optimum stacking sequences for maximum fundamental frequency and maximum frequency separation of symmetric hybrid laminates undergoing free vibrations. They neglected the bending-twisting effects but in order to avoid an excessive error, they imposed special constraints on bending stiffness terms. They restricted the fiber orientations to preselected four different angles to save from computational time.

In many of the previous studies, in order to find the optimum design, gradient-based search techniques [4-5] or enumeration (trial of all configurations) [7] were used as optimization methods. Narita [10] proposed a layerwise optimization method to maximize natural frequency of laminated plates. The optimum angles were found from outer layer to inner layer with one-dimensional search in order to save time. Enumeration, which is the most reliable one, takes a very long time and becomes infeasible for large design spaces. Deterministic algorithms are sensitive to starting point and they most probably converge to a local minimum in complex design spaces. This is the reason why many of the previous researchers [1-5, 7] imposed many limitations on ply numbers and angle orientations.

Because the search algorithms were usually suitable only for continuous optimization variables, design optimization of composite laminates was usually formulated as a continuous optimization problem [1-6, 9] such that ply thicknesses and orientation angles were taken as continuous variables. Since laminates are stack of plies with a given thickness, ply thicknesses of the final designs had to be rounded to the nearest discrete

value. Fiber orientations had also to be chosen among usable angles due to manufacturing constraints. After rounding off the values of continuous design variables, the resulting design may not be an optimum design and the constraints may even be violated. For these reasons, optimization of composites should be formulated as a discrete optimization problem [7-8, 10-16].

Because of high material cost of composite structures, optimization algorithms capable of finding the most effective use of material should be utilized. Stochastic search algorithms are better alternatives to traditional search techniques because they can find the globally optimal configuration without being sensitive to starting point by searching a larger solution domain, they are suitable for discrete optimization problems, and they do not need derivatives of objective function. They have been used successfully in optimization problems having complex design spaces. Genetic algorithms and simulated annealing algorithms (SA) are the popular stochastic algorithms. For composite optimization, researchers mostly preferred to use genetic algorithms [11-14] rather than simulated annealing algorithms [15-16]. The main advantage of genetic algorithm is preservation of a population of current configurations while simulated annealing preserves only one configuration. However, some variants of SA like direct search simulated annealing incorporated this property.

Objective function of the optimization problem should be accurately calculated during an optimization process to avoid spurious optimum points. In some studies of frequency optimization, the researchers imposed some restrictions on fiber orientations to avoid excessive errors in the frequency results caused by bending-twisting effects. Bert [1-2] used a balanced laminate and Rao and Singh [6] used an orthotropic laminate for the optimization problem. These restrictions, however, might prevent finding much better designs. For this reason, in an efficient design optimization, there should be no limitation on fiber orientations except the ones due to manufacturing and design requirements. Besides, the method used to evaluate natural frequency should not yield incorrect results for any arbitrary laminate configuration. Structural analysis of laminated composite plates is more complex than the isotropic plates because of the anisotropy of each layer so additional care must be taken for designing the composite plates. Natural frequencies of rectangular laminated plates can be calculated with either approximate or exact solution

methods. Approximate methods especially Rayleigh-Ritz method and finite element method were preferred in the previous studies [11-14] that used stochastic search techniques.

If the solution for natural frequency is obtained by the traditional analytical approaches like Navier's method, the natural boundary conditions cannot be satisfied in the presence of bending-twisting coupling. Whitney and Leissa [17] tried to solve the bending, free vibration and buckling problems for anisotropic laminates and obtained closed-form solutions only for limited types of laminates. The traditional analytical approaches can find solution only for a few specific types of stacking sequences having no bending-twisting coupling.

Chaudhuri [18-19] presented another analytical approach called "boundary displacement double Fourier series method". In this method, the geometric boundary conditions are satisfied as well as the natural boundary conditions unlike Navier's approach. This method was proposed for the solution of completely coupled linear second order partial differential equations by Chaudhuri [18] and for the solution of completely coupled linear rth order partial differential equations by Chaudhuri [19] with constant coefficients subjected to completely coupled boundary conditions.

This method is suitable for the solution of free vibration and buckling problems of symmetric anisotropic plates, which have a completely coupled linear fourth order governing equation. Using this method, Green [20] presented the solution of buckling and free vibration problems for isotropic plates. Green and Hearmon [21] solved the buckling problem of a thin anisotropic rectangular plate with simply supported edges. Whitney [22] used the same method for bending, free vibration and buckling problems of symmetric laminated plates with clamped and simply supported edges [23]. Whitney and Leissa [24] solved bending, free vibration and buckling problem of unsymmetric laminated plates with simply supported edges. Recently by using the boundary-continuous-displacement type Fourier series method, Chaudhuri et al. [25] presented a solution for the free vibration problem of symmetric rectangular anisotropic laminates. He obtained a closed form solution for simply supported edges available for all fiber orientations like Green and Hearmon [21].

The objective of the present study is to find the optimum stacking sequence, which gives the maximum natural frequency or maximum frequency separation for laminated plates. In this study, the boundary-continuous-displacement type Fourier series method [19-25] is employed to calculate the natural frequency of the laminated plates and an enhanced version of simulated annealing, direct simulated annealing, developed by Ali et al. [26], is used as the optimization algorithm. It is different from the previous studies in two aspects: Firstly, it is the first study that uses an analytical method instead of an approximate method to calculate the frequency response of laminates including bending-twisting coupling. In this way, no restrictions on ply angles are imposed to avoid error in calculation. Secondly, this is one of the rare studies that use the simulated annealing algorithm for laminated plate optimization. Since this is a reliable global search algorithm, globally optimal designs for very complex problems could be obtained in this study.

2. PROBLEM STATEMENT

In this study, out-of-plane free vibration response of simply supported rectangular laminated plates (Figure 2.1) is considered.

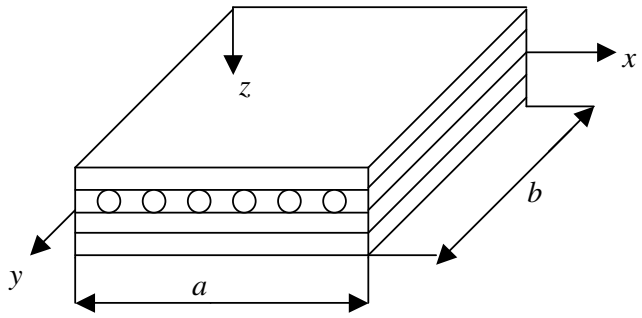

Figure 2.1. A rectangular laminated plated consisting of multiple lamina

Its plies are symmetrically arranged about the middle surface. Design variables are the fiber orientation angles in the upper (or lower) layers of the laminate with respect to the mid-plane. They are constrained to have discrete values due to manufacturing requirements; but no other restrictions are imposed. The thickness of each layer is the same and not varied during optimization.

The first problem is to find the optimum configuration of a composite laminate having the maximum fundamental frequency with a predetermined number of layers, *n*.

$$\text{Maximize } \Omega_1 (\theta_1, \theta_2, \theta_3 \ldots \theta_n)$$

$$\text{where } \Omega_1 (\theta_1, \theta_2, \theta_3 \ldots \theta_n) = \text{minimum of } \Omega_{rs} (\theta_1, \theta_2, \theta_3 \ldots \theta_n) \tag{2.1}$$

$$\text{Subject to } \quad -90 \le \theta_k \le 90 \qquad \text{where } k = 1, 2 \ldots . n \tag{2.2}$$

Ω_i are the natural frequencies, which are the eigenfrequencies corresponding to the eigenmodes (r,s) and Ω_1 is the smallest one, which is called the fundamental frequency.

The second problem is to find the optimum configuration with maximum separation between two adjacent frequencies, which is called frequency separation problem.

$$\text{Maximize } (\Omega_{i+1}(\theta_1, \theta_2, \theta_3 \ldots \theta_n) - \Omega_i (\theta_1, \theta_2, \theta_3 \ldots \theta_n)) \quad i = 1,2 \tag{2.3}$$

$$\text{Subject to } -90 \leq \theta_k \leq 90 \qquad \text{where } k = 1, 2 \ldots . n \tag{2.4}$$

where Ω_2 is the next lowest frequency and Ω_3 is the third lowest frequency.

3. ANALYSIS OF LAMINATED PLATES

Stress-strain, strain-displacement relations and stress resultant definitions yield the following relation

$$\begin{bmatrix} N_x \\ N_y \\ N_{xy} \\ M_x \\ M_y \\ M_{xy} \end{bmatrix} = \begin{bmatrix} A_{11} & A_{12} & A_{16} & B_{11} & B_{12} & B_{16} \\ A_{12} & A_{22} & A_{26} & B_{12} & B_{22} & B_{26} \\ A_{16} & A_{26} & A_{66} & B_{16} & B_{26} & B_{66} \\ B_{11} & B_{12} & B_{16} & D_{11} & D_{12} & D_{16} \\ B_{12} & B_{22} & B_{16} & D_{12} & D_{22} & D_{26} \\ B_{16} & B_{26} & B_{66} & D_{16} & D_{26} & D_{66} \end{bmatrix} \begin{bmatrix} \varepsilon_x^{\,0} \\ \varepsilon_y^{\,0} \\ \gamma_{xy}^{\,0} \\ \kappa_x \\ \kappa_y \\ \kappa_{xy} \end{bmatrix} \tag{3.1}$$

where the laminate extensional stiffness terms are given by

$$A_{ij} = \sum_{k=1}^{N} (\overline{Q}_{ij})_k (z_k - z_{k-1}) \tag{3.2}$$

the laminate coupling stiffness terms are given by

$$B_{ij} = \frac{1}{2} \sum_{k=1}^{N} (\overline{Q}_{ij})_k (z_k^{\,2} - z_{k-1}^{\,2}) \tag{3.3}$$

the laminate bending stiffness terms are given by

$$D_{ij} = \frac{1}{3} \sum_{k=1}^{N} (\overline{Q}_{ij})_k (z_k^{\,3} - z_{k-1}^{\,3}) \tag{3.4}$$

where z_k is the coordinate of the top of the kth layer counted from the mid-plane and $(\overline{Q}_{ij})_k$ are the stiffness terms for the kth layer with respect to an arbitrary in-plane coordinates and they are constant in each layer.

$$\begin{bmatrix} \sigma_x \\ \sigma_y \\ \tau_{xy} \end{bmatrix}_k = \begin{bmatrix} \overline{Q}_{11} & \overline{Q}_{12} & \overline{Q}_{16} \\ \overline{Q}_{12} & \overline{Q}_{22} & \overline{Q}_{26} \\ \overline{Q}_{16} & \overline{Q}_{26} & \overline{Q}_{66} \end{bmatrix}_k \begin{bmatrix} \varepsilon_x \\ \varepsilon_y \\ \gamma_{xy} \end{bmatrix} \tag{3.5}$$

$(\overline{Q}_{ij})_k$ can be expressed in terms of the stiffness components $(Q_{ij})_k$ in principal directions:

$$\overline{Q}_{11} = Q_{11}\cos^4\theta + 2(Q_{12} + 2Q_{66})\sin^2\theta\cos^2\theta + Q_{22}\sin^4\theta \tag{3.6}$$

$$\overline{Q}_{12} = (Q_{11} + Q_{22} - 4Q_{66})\sin^2\theta\cos^2\theta + Q_{12}(\sin^4\theta + \cos^4\theta) \tag{3.7}$$

$$\overline{Q}_{22} = Q_{11}\sin^4\theta + 2(Q_{12} + 2Q_{66})\sin^2\theta\cos^2\theta + Q_{22}\cos^4\theta \tag{3.8}$$

$$\overline{Q}_{16} = (Q_{11} - Q_{12} - 2Q_{66})\sin\theta\cos^3\theta + (Q_{12} - Q_{22} + 2Q_{66})\sin^3\theta\cos\theta \tag{3.9}$$

$$\overline{Q}_{26} = (Q_{11} - Q_{12} - 2Q_{66})\sin^3\theta\cos\theta + (Q_{12} - Q_{22} + 2Q_{66})\sin\theta\cos^3\theta \tag{3.10}$$

$$\overline{Q}_{66} = (Q_{11} + Q_{22} - 2Q_{12} - 2Q_{66})\sin^2\theta\cos^2\theta + Q_{66}(\sin^4\theta + \cos^4\theta) \tag{3.11}$$

The principal stiffness terms, Q_{ij}, are related to the elastic properties of the material along the principal directions, E_1, E_2, G_{12}, ν_{12}, and ν_{21}. More detailed information is provided in Jones [27].

From the Eqs. (3.9) and (3.10), it can be inferred that

$$(\overline{Q}_{16})_{+\theta} = -(\overline{Q}_{16})_{-\theta} \tag{3.12}$$

$$(\overline{Q}_{26})_{+\theta} = -(\overline{Q}_{26})_{-\theta} \tag{3.13}$$

Jones [27] defined the antisymmetric angle-ply laminate as a laminate having laminae oriented at +θ degrees to the laminate coordinate axes on one side of the middle surface and corresponding equal-thickness laminae oriented at –θ degrees on the other side at the same distance from the middle surface. Because antisymmetric laminates are not symmetric, the coupling stiffness terms, B_{ij}, do not vanish.

With the help of Eqs. (3.4), (3.12) and (3.13) it can be stated that for antisymmetric angle-ply laminates there is no bending-twisting coupling, which means

$$D_{16} = 0 \quad \text{and} \quad D_{26} = 0 \tag{3.14}$$

Jones [27] called the specially orthotropic lamina as a laminate made of a stack of orthotropic laminae whose principal material axes are aligned with the laminate coordinate axes. This means the orientation angles of the fibers are either 0° or 90°. For a laminate which has multiple specially orthotropic layers, Eqs. (3.9) and (3.10) imply that

$$\overline{Q}_{16} = 0 \text{ and } \overline{Q}_{26} = 0 \tag{3.15}$$

and from the Eq. (3.4), one may conclude that there is also no bending-twisting coupling:

$$D_{16} = 0 \quad \text{and} \quad D_{26} = 0 \tag{3.16}$$

Other than these two types of laminate configurations, practically there is no laminate configuration in which bending-twisting coupling does not exist. This means a very limited class of laminates has no bending-twisting coupling.

In this thesis, laminates whose principal material axes are not aligned with the laminate coordinate axes are called anisotropic as in Whitney and Leissa [17], Whitney [22-23], Whitney and Leissa [24], Chaudhuri et al. [25].

The in-plane force resultants develop due to out-of-plane deformation for unsymmetrical laminates, where coefficients of bending-extension coupling, $B_{ij,}$ are

nonzero as seen in Eq. (3.1). The in-plane displacements u^0 and v^0 are coupled with the transverse displacements, w, when the coupling stiffness terms, $B_{ij,}$ are present.

The coupled differential equation for free vibration of laminated plate is given below. More detailed information is provided in Appendix A.

$$\begin{aligned} &D_{11}\frac{\partial^4 w}{\partial x^4}+4D_{16}\frac{\partial^4 w}{\partial x^3\partial y}+2(D_{12}+2D_{66})\frac{\partial^4 w}{\partial x^2\partial y^2}+4D_{26}\frac{\partial^4 w}{\partial x\partial y^3}+D_{22}\frac{\partial^4 w}{\partial y^4}\\ &-B_{11}\frac{\partial^3 u^0}{\partial x^3}-3B_{16}\frac{\partial^3 u^0}{\partial x^2\partial y}-(B_{12}+B_{66})\frac{\partial^3 u^0}{\partial x\partial y^2}-B_{26}\frac{\partial^3 u^0}{\partial y^3}-B_{16}\frac{\partial^3 v^0}{\partial x^3}\\ &-(B_{12}+2B_{66})\frac{\partial^3 v^0}{\partial x^2\partial y}-3B_{26}\frac{\partial^3 v^0}{\partial x\partial y^2}-B_{22}\frac{\partial^3 v^0}{\partial y^3}=-\rho_0 h\frac{\partial^2 w}{\partial t^2}\end{aligned} \tag{3.17}$$

For symmetrically laminated plates, the coupling between in-plane and out of plane behaviors vanishes, $B_{ij} = 0$, Eq. (3.17) reduces to

$$\begin{aligned} &D_{11}\frac{\partial^4 w}{\partial x^4}+4D_{16}\frac{\partial^4 w}{\partial x^3\partial y}+2(D_{12}+2D_{66})\frac{\partial^4 w}{\partial x^2\partial y^2}\\ &+4D_{26}\frac{\partial^4 w}{\partial x\partial y^3}+D_{22}\frac{\partial^4 w}{\partial y^4}=-\rho_0 h\frac{\partial^2 w}{\partial t^2}\end{aligned} \tag{3.18}$$

The differential equation in Eq. (3.18) is to be solved for the boundary conditions applied on the edges. In this study, simply supported edge conditions were considered. For simply supported edges, transverse displacement and bending moment are set to zero. For symmetric laminates, for which $B_{ij} = 0$, moment resultants depend only on curvatures. Then the boundary conditions for simply supported edges are given as follows

$$w = 0 \quad \text{and} \quad M_x=-\left(D_{11}\frac{\partial^2 w}{\partial x^2}+2D_{16}\frac{\partial^2 w}{\partial x\partial y}+D_{12}\frac{\partial^2 w}{\partial y^2}\right)=0 \qquad \text{for x = 0, a} \tag{3.19}$$

$$w = 0 \quad \text{and} \quad M_y=-\left(D_{12}\frac{\partial^2 w}{\partial x^2}+2D_{26}\frac{\partial^2 w}{\partial x\partial y}+D_{22}\frac{\partial^2 w}{\partial y^2}\right)=0 \qquad \text{for y = 0, b} \tag{3.20}$$

4. NATURAL FREQUENCY ANALYSIS OF LAMINATED PLATES

Boundary-continuous-displacement double Fourier series method (Chaudhuri [19]) was employed to solve the governing differential equation for natural frequencies of rectangular thin laminated plates. For the natural frequency problem of arbitrarily laminated plates, it is not possible to satisfy all the boundary conditions and establish a solution with the general continuous Fourier series. However, if proper discontinuities are added to the assumed solution function and its derivatives at the boundaries, all of the boundary conditions can be satisfied and a solution can be obtained. Therefore, in addition to unknown Fourier coefficients of the complete solution, additional Fourier coefficients coming from the discontinuities added to the assumed solution functions and their derivatives at the boundaries are included to the system.

After differentiating the assumed solution function in the presence of discontinuities, they are substituted into the governing partial differential equation and into the boundary conditions to establish the solution. For the given problem, the governing equation is given in Equation (3.18) and the boundary conditions are given in Equations (3.19) and (3.20). Then, the coupled partial differential equation of motion is reduced to the following set of equations:

$$F(r,s)\,V_{rs} - 2\sum_{m=1}^{\infty}\sum_{n=1}^{\infty}\alpha_m\,\beta_n\left\{\gamma(\alpha_m{}^2+\alpha_r{}^2)+\chi\left(\beta_s{}^2+\beta_n{}^2\right)\right\}h_{rm}\,h_{sn}\,V_{mn}=0 \tag{4.1}$$

$$F(r,s)=\alpha_r{}^4+2\zeta\alpha_r{}^2\beta_s{}^2+\eta\beta_s{}^4-\lambda \tag{4.2}$$

$$\alpha_r=\frac{r\pi}{a}\quad,\qquad \beta_s=\frac{s\pi}{b} \tag{4.3}$$

$$\zeta=\frac{(D_{12}+2D_{66})}{D_{11}}\;,\quad \eta=\frac{D_{22}}{D_{11}}\;,\quad \lambda=\frac{\bar{\rho}\omega^2}{D_{11}}\;,\quad \gamma=\frac{D_{16}}{D_{11}}\;,\quad \chi=\frac{D_{26}}{D_{11}} \tag{4.4}$$

$$h_{rm} = \begin{cases} \dfrac{4m}{\pi(m^2 - r^2)}, & m + r = \text{odd} \\ 0, & m + r = \text{even} \end{cases} \tag{4.5}$$

$$h_{sn} = \begin{cases} \dfrac{4n}{\pi(n^2 - s^2)}, & n + s = \text{odd} \\ 0, & n + s = \text{even} \end{cases} \tag{4.6}$$

where m, n, r, s are the indices of the Fourier series, V_{mn} are the plate Fourier coefficients, D_{ij} are the bending stiffness terms, a and b are the length and the width of the rectangular plate, $\overline{\rho}$ is the mass density of the plate material per unit area and ω is the natural frequency of the laminate. Details can be found in Chaudhuri et al. [25] and the whole solution procedure can be found in Appendix A.

Expanding Equation (4.1) with a certain number of terms in Fourier series leads to a system of equations, which may be expressed in matrix form. The size of this matrix depends on the number of the terms taken from the Fourier series. Eigenvalues corresponding to different modes can be found by setting the determinant of this matrix to zero. Fundamental frequency, which is the lowest of all the natural frequencies, always occurs when the eigenmode (r,s) is equal to (1,1).

4.1. Testing the Convergence of the Method

No convergence tests for frequency analyses were found in the literature for free vibration of anisotropic laminates calculated with the boundary-continuous-displacement double Fourier series method. In this study, convergence tests were conducted to determine how many Fourier series terms were sufficient to obtain the desired accuracy.

In the convergence tests, the material properties (Table 4.1) and the laminate configurations given by Narita [10], Cupial [28] and Leissa and Narita [29] were used.

Table 4.1. Material properties for graphite-epoxy [10, 28, 29]

E_{11}	138 GPa
E_{22}	8.96 GPa
G_{12}	7.1 GPa
υ_{12}	0.3

In these studies, a frequency parameter was defined by normalizing the natural frequency as

$$\Omega = \omega a^2 \sqrt{\frac{\overline{\rho}}{D_0}} \tag{4.7}$$

where ω is frequency, a is the length of the rectangular plate, $\overline{\rho}$ is mass density of the plate material per unit area. D_0 is a reference bending stiffness defined by

$$D_0 = \frac{E_1 h^3}{12\,(1-\nu_{12}\nu_{21})} \tag{4.8}$$

where ν is Poisson's ratio, E_1 is the Young's modulus in longitudinal direction and h is the height of the laminate. Instead of D_{ij} (i,j = 1,2,6), D_o is used in the definition of the frequency parameter because it does not change with the change of fiber orientations. Because frequency is normalized with the height of the laminate, direct comparison can be made between laminates having different number of layers.

Narita [10] used a rectangular eight-layered plate with a symmetric lay-up, $[45/-45_3]_s$, and an aspect ratio being equal to one. Figure 4.1 shows the convergence of the boundary-continuous-displacement double Fourier series method for this laminate configuration.

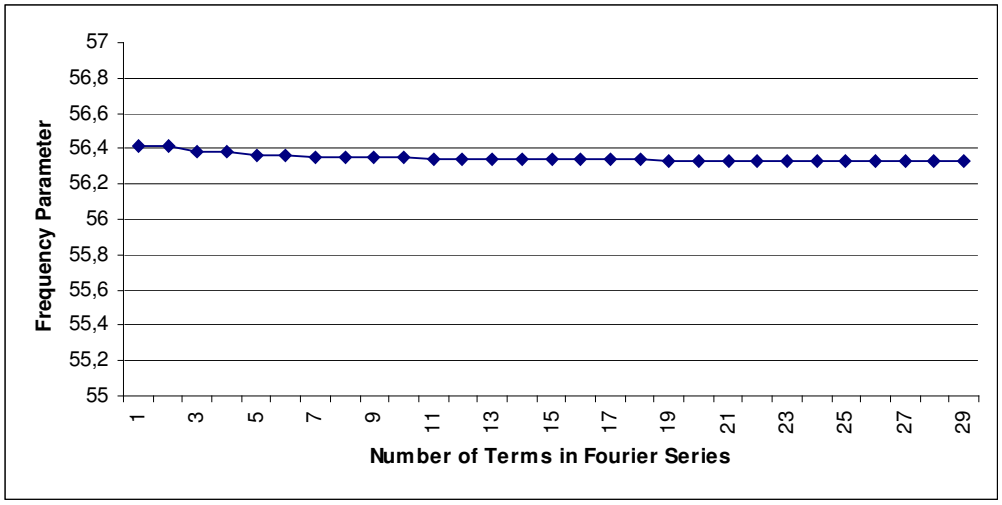

Figure 4.1. Convergence of the frequency parameter of the laminate

Cupial [28] and Leissa and Narita [29] used a rectangular 30° one-layered plate with an aspect ratio of one. Figure 4.2 shows the convergence of the boundary-continuous-displacement double Fourier series method for the given laminate.

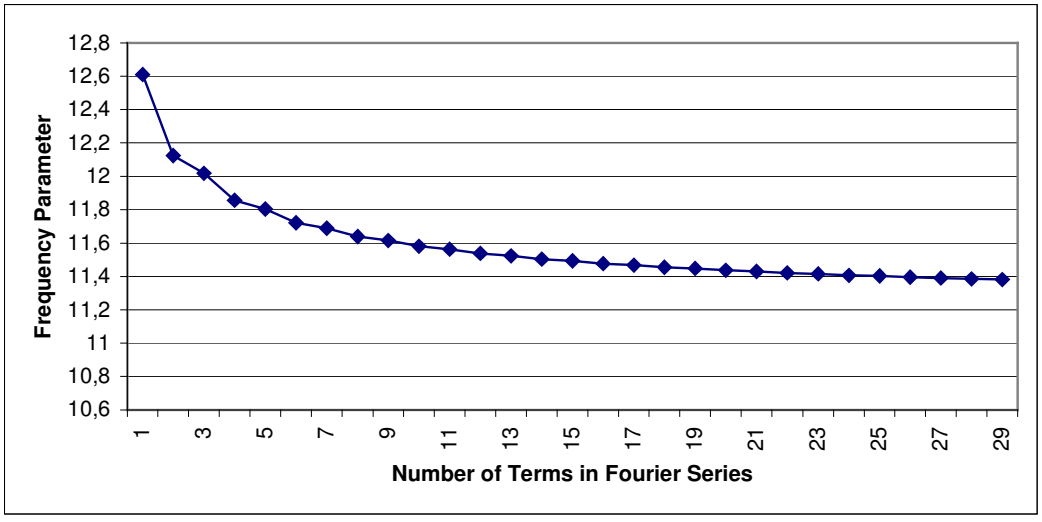

Figure 4.2. Convergence of the vibration response of the laminate

The graphs imply that the frequency parameter can be accurately calculated if 10-15 terms are included and after 20 terms its value remains about the same. Accordingly, natural frequency calculations were carried out with the first 20 terms of the Fourier series

4.2. Comparison of the Frequency Analysis Results

The results of the analytical frequency model used in this study in terms of frequency parameter (Equation (4.7)) were compared with the ones obtained in previous studies. Table 4.2 shows the frequency parameters corresponding to the first six modes calculated with 16 and 20 terms of the Fourier series for same material properties and laminate lay-up used in the convergence test.

Table 4.2. Comparison of the frequency parameter values

	Mode					
	1	2	3	4	5	6
Present (16 terms)	11.492	20.699	33.457	35.279	47.994	49.010
Present (20 terms)	11.447	20.597	33.368	35.205	47.841	48.870
Reference [28]	11.264	20.307	33.000	34.920	47.247	48.353
Reference [29]	11.69	21.00	33.91	35.62	48.72	49.78

Both of the references [28-29] in Table 4.2 used Ragleigh-Ritz method with (8x8) polynomials including bending-twisting effects. Cupial [28] used orthogonal polynomials and Leissa and Narita [29] used double-sine series. As seen in the table, the results obtained by the frequency analysis used in this study are very close to the results provided

in the literature. The differences may be attributed to the use of different models and the number of terms used in approximations.

5. OPTIMIZATION METHOD

The name of simulated annealing comes from the physical annealing process. Annealing process is used for obtaining regular crystal configuration with minimum number of defects. In this technique, solid is heated to high temperatures, and then it is cooled slowly. Mobility of atoms increases with the increasing temperature and during cooling atoms tend to form most possible regular arrangements. Temperature must be decreased by slow stages and at each stage thermal equilibrium must be obtained. Slow cooling gives the atoms more chances to arrange regularly and form a crystalline configuration with a lower energy state. At the end of the annealing process, the final configuration has minimum number of defects.

In simulated annealing randomly generated configurations are renewed through iterations while the temperature parameter is gradually decreased. Firstly, an initial configuration is chosen randomly. At each iteration, a new configuration is generated randomly in the neighborhood of the current point. Cost of the point is determined from the objective function. Then, the algorithm compares the cost of the new point to the cost of the current point. If the new point is better than the current one, it is always accepted. Then the current point is substituted to the newer one and the new point becomes the current one. Otherwise, non-improving solution is chosen with a probability that depends on the temperature parameter and cost difference between the current point and the new point. Once a new point is accepted, it replaces the current point. For a number of trials, the temperature parameter is kept constant and then it is gradually decreased during the optimization process. Slow cooling and accepting a worse solution serve the purpose of escaping local optima.

In the present study, direct simulated annealing (DSA) proposed by Ali et al. [26], which is an enhanced version of simulated annealing, was adopted. It uses a set of current configurations rather than a single configuration as in the SA algorithm. If the new configuration is accepted, it substitutes the worst current configuration so the best configuration is always kept. In ordinary simulated annealing, many good configurations are lost when they are replaced by worse configurations especially at the early stages of

optimization. In a way, this feature of DSA adds a kind of memory to the optimization procedure and thus prevents losing good configurations unless better ones are generated.

The objective functions of the optimization problem considered in this study are the fundamental frequency of the laminate and the frequency difference of the two adjacent frequencies. The configuration to be optimized is the stacking sequence of the laminate having different angle orientations at each layer. Design variables are then discrete fiber orientation angles. By randomly changing the orientation angles, different configurations can be obtained randomly.

5.1. Application of DSA Algorithm to the Frequency Optimization Problem

Firstly, N number of configurations are created at the beginning of the optimization process. N depends on the dimension of the problem, n, i.e. number of design variables. In the present problem, the dimension, n, is equal to the number of distinct fiber angles. Since the laminate is symmetric, n is actually equal to the half of the total number of layers. Ali et al. [26] tested the algorithm for different configuration numbers such as N being equal to $5(n+1)$ $7(n+1)$, $10(n+1)$ and compared the number of function evaluations, number of failures and computational times. The reliability of the algorithm increases with increasing number of configuration numbers at the expense of computational time. They chose the appropriate number of initial configurations as

$$N = 7\ (n+1) \tag{5.1}$$

The initial configurations are generated by randomly choosing lamina angles between –90° and 90°.

Because fiber orientation angles should be discrete due to manufacturing requirements, generated angle values are rounded to the closest chosen discrete angle. The designer decides on the angle increments, which may be 30º, 15º, 10º, 5º, 1º or even less, according to the manufacturing precision or easiness.

In each iteration, a new configuration is generated randomly in the neighborhood of a randomly chosen current configuration. This is achieved by first randomly choosing one of the current configurations and then introducing random variations to its lamina angles. The new lamina angle of the kth layer, θ_k' , is calculated as

$$\theta_k' = \theta_k + r\,\Delta\theta_{\max} \tag{5.2}$$

where r is a randomly chosen real number between -1.0 and 1.0 ($r \in \Re : -1 \le r \le 1$), θ_k is the current angle of the kth layer, and $\Delta\theta_{\max}$ is the maximum angle variation. If the angles fall outside of the interval, they are modified according to

$$\theta_k'' = \begin{Bmatrix} \theta_k' - 180 & if & \theta_k' > 90 \\ \theta_k' + 180 & if & \theta_k' < -90 \\ \theta_k' & if & -90 \le \theta_k' \le 90 \end{Bmatrix} \tag{5.3}$$

where θ_k'' is modified angle value.

When a new configuration is generated, it is compared with the worst current design to decide on whether it will be accepted or not. It is then either accepted or rejected according to the acceptance criterion of the simulated annealing algorithm. Acceptability is based on the following formula:

$$A_t = \begin{Bmatrix} 1 & if & f_t \le f_h \\ \exp\left(-\left(f_t - f_h\right) / T_k\right) & if & f_t > f_h \end{Bmatrix} \tag{5.4}$$

where f_t is the cost of the trial design, f_h is the highest cost of the N number of current configurations, T_k is the temperature parameter for the kth Markov chain. A Markov chain is a sequence of trials accomplished at the same temperature. If A_t is greater than a randomly generated number P_r, then the new configuration is accepted, otherwise it is rejected. The acceptance probability for configurations that are worse than the worst current configuration is high at high temperatures as the formula implies. It decreases with the decreasing temperature and in the end worse designs are almost never allowed.

The length of a Markov chain depends on the dimension of the problem *n*, and the difference between the highest and lowest costs of the current designs. According to Ali et al. [26], the length of the kth Markov chain is calculated as

$$L_k = L + L\left\{1 - \exp(-(f_h - f_l))\right\} \tag{5.5}$$

where

$$L = 10\,n \tag{5.6}$$

If the difference between the highest cost and the lowest cost at a certain temperature increases, the length of Markov chain and thus the number of iterations increase. If a point which has a lower cost than the best point is found, then the Markov chain is not executed any more and a new one begins.

At the beginning of the algorithm, the temperature parameter must be relatively high. In order to prevent getting stuck into a local minimum at early stage of the optimization, the probability of acceptability must be high. That means, acceptance ratio that is defined as the ratio between the number of accepted trials and total number of trials should be close to one.

During optimization, the temperature is lowered in order to obtain shrinking. The temperature parameter should be decreased gradually so that a large part of the solution domain can be searched without getting stuck to a local minimum. The temperature in the (k+1)th Markov chain is calculated as

$$T_{k+1} = \alpha_{k+1} T_k \tag{5.7}$$

where T_k is the temperature parameter in the kth Markov chain and the coefficient α_{k+1} is calculated as

$$\alpha_{k+1} = \begin{Bmatrix} \alpha_{\max} & if & L_k > L'_k \\ a_k - (a_k - a_{\min})(1 - L'_{k-1}/L_k) & else\ if & L_k > L'_{k-1} \\ a_{\max} - (a_{\max} - a_k)(L_k / L'_{k-1}) & else & L_k \le L'_{k-1} \end{Bmatrix} \tag{5.8}$$

where L'_k denotes the actual number of trials executed in the kth Markov chain whose length is L_k. If the best point is changed during the Markov chain, it is stopped and L'_k is equated to the number of trials executed. Otherwise, L'_k is set to the value of L_k. $\alpha_{\max}$ and $\alpha_{\min}$ are constants. The temperature is reduced very slowly. In this study, the values $\alpha_{\max} = 0.9997$ and $\alpha_{\min} = 0.999$ were chosen.

At the beginning of the optimization, a large value (50.0) is chosen for the maximum angle variation in order to search a large solution domain, which is then reduced in later stages. This means that at initial stages, the neighborhood of the current configurations, where a better configuration is searched, is large. With the progression of optimization, improvements in the current configurations become scarce. The worse current configuration is defined as the one, which is worse than all of the current configurations except the worst one. If there is no improvement on the worse design during a Markov chain, $\Delta\theta_{\max}$ is reduced to make the searched region smaller and thus increase the likelihood of finding a better design. This is similar as the physical annealing process. At the beginning, when the temperature is high, atoms are disorderly positioned and their mobility is high so they are able to move to a large distance. During cool down, the movements of the atoms become slow so they can make only small-scale arrangements.

Initially, the current configurations are dispersed over the design domain. But towards the end of the optimization, they cluster around a few points, supposedly around the multiple global optimums or near global optimums, and the difference between the best and the worst cost becomes very small. At this stage, one may assume that the optimization process has converged to the optimum design(s). The stopping criterion for the algorithm may then be expressed as

$$f_h - f_l \le \varepsilon \tag{5.9}$$

6. RESULTS

6.1. Comparison of the Optimization Results for Fundamental Frequency Maximization

The results of the optimization procedure proposed in this study for maximizing natural frequency were compared with that of previous studies. Comparisons were made with the numerical results provided by Reiss and Ramachandran [3], Mateus et al. [4] and Soares et al. [5] for a rectangular four-layered plate with a symmetric balanced lay-up $[\theta/-\theta]_s$. Reiss and Ramachandran [3] used a closed form solution for the frequency of the laminate. Mateus et al. [4] and Soares et al. [5] used finite element method to determine the frequency response and gradient-based search techniques to determine the optimum results. The material properties that they used are given in Table 6.1.

Table 6.1. Material properties for graphite-epoxy [3-5]

E_{11}	200 GPa
E_{22}	20 GPa
G_{12}	5 GPa
ν_{12}	0.3

Table 6.2 shows the optimum angles that maximize the fundamental frequency of the laminate with different aspect ratios. *a* and *b* are the lateral dimensions of the plate. Discrete 1° angle increment is used. As seen in the table, the results are quite similar. Because the laminate configuration is defined through a single design variable, the globally optimum design can even be found by using a local search algorithm. For this reason, the advantage of using a global search algorithm is not apparent for this configuration.

Table 6.2. Comparison of the optimum angles obtained in this study and previously for frequency maximization

	a / *b*				
	1.0	1.2	1.3	1.7	2.0
Present	45° Ω = 42.67	51° Ω = 52.15	56° Ω = 57.75	90° Ω =127.68	90° Ω =127.68
Reference [3]	45°	49.4°	54.7°	90°	_
Reference [4]	45°	50.6°	54.4°	90°	89.7°
Reference [5]	45°	50.9°	55°	89.8°	89.6°

6.2. Comparison of the Optimization Results for Frequency Separation

Adali and Verijenko [7] considered problems of separation between the first and the second frequencies and between the second and the third frequencies. They optimized symmetric laminates having 4, 8, 12 and 16 plies with an aspect ratio of 2.0. Each symmetric ply pair might have a different fiber angle. Therefore, up to eight different fiber angles were used as design variables. These angles might take only four different discrete values {0°, -45°, 45°, 90°}. They used T300/5280 graphite-epoxy and Scotchply 1002 glass-epoxy with the material properties given in Tables 6.3 and 6.4. Their optimization results and the results of the present study are given in Tables 6.5-6.8. $\Delta\Omega_{ij}$ is the difference between the frequency parameters Ω_i and Ω_j corresponding to natural frequencies ω_i and ω_j as defined in Eq. (4.7).

Table 6.3. Material properties for T300/5280 graphite-epoxy [7]

E_{11}	181 GPa
E_{22}	10.3 GPa
G_{12}	7.17 GPa
ν_{12}	0.28

Table 6.4. Material properties for Scotchply 1002 glass-epoxy [7]

E_{11}	38.6 GPa
E_{22}	8.27 GPa
G_{12}	4.14 GPa
ν_{12}	0.26

Table 6.5. Optimum angles for frequency separation $\Delta\Omega_{12}$ for graphite-epoxy

Number of Plies	**Optimum Configuration Reference [7]**	**Optimum Configuration Present**	**Ω_1 and Ω_2 Present**	**$\Delta\Omega_{12}$ Present**
4	$[45/0]_s$	$[0_2]_s$	Ω_1= 67.59 Ω_2 = 178.44	$\Delta\Omega_{12}$ = 110.85
8	$[45/0_3]_s$	$[45/0_3]_s$	Ω_1= 69.23 Ω_2 = 183.84	$\Delta\Omega_{12}$ = 114.61
12	$[0/45/0_4]_s$	$[90/0_5]_s$	Ω_1= 68.42 Ω_2 = 183.71	$\Delta\Omega_{12}$ = 115.29 (For $[0/45/0_4]_s$ $\Delta\Omega_{12}$ = 114.64)
16	$[90/45/0_6]_s$	$[90/45/0_6]_s$	Ω_1= 69.38 Ω_2 = 184.75	$\Delta\Omega_{12}$ = 115.37

Table 6.6. Optimum angles for frequency separation $\Delta\Omega_{23}$ for graphite-epoxy

Number of Plies	**Optimum Configuration Reference [7]**	**Optimum Configuration Present**	**Ω_2 and Ω_3 Present**	**$\Delta\Omega_{23}$ Present**
4	$[90/0]_s$	$[45/-45]_s$	$\Omega_2 = 208.90$ $\Omega_3 = 320.49$	$\Delta\Omega_{23} = 111.59$ (For $[90/0]s$ $\Delta\Omega_{23} = 103.85$)
8	$[0_2/90/0]_s$	$[0_2/90/0]_s$	$\Omega_2 = 184.77$ $\Omega_3 = 347.48$	$\Delta\Omega_{23} = 162.71$
12	$[90_2/45/90/0_2]_s$	$[0/90/45/90/0_2]_s$	$\Omega_2 = 189.60$ $\Omega_3 = 358.23$	$\Delta\Omega_{23} = 168.63$ (For $[90_2/45/90/0_2]s$ $\Delta\Omega_{23} = 168.19$)
16	$[0/-45/90_3/0_3]_s$	$[0/-45/90_3/0_3]_s$	$\Omega_2 = 185.63$ $\Omega_3 = 357.45$	$\Delta\Omega_{23} = 171.82$

Table 6.7. Optimum angles for frequency separation $\Delta\Omega_{12}$ for glass-epoxy

Number of Plies	**Optimum Configuration Reference [7]**	**Optimum Configuration Present**	**Ω_1 and Ω_2 Present**	**$\Delta\Omega_{12}$ Present**
4	$[0_2]_s$	$[0_2]_s$	Ω_1= 54.63 Ω_2 = 112.78	$\Delta\Omega_{12}$ = 58.15
8	$[0_4]_s$	$[0_4]_s$	Ω_1= 54.63 Ω_2 = 112.78	$\Delta\Omega_{12}$ = 58.15
12	$[0_6]_s$	$[0_6]_s$	Ω_1= 54.63 Ω_2 = 112.78	$\Delta\Omega_{12}$ = 58.15
16	$[0_8]_s$	$[0_8]_s$	Ω_1= 54.63 Ω_2 = 112.78	$\Delta\Omega_{12}$ = 58.15

Table 6.8. Optimum angles for frequency separation $\Delta\Omega_{23}$ for glass-epoxy

Number of Plies	**Optimum Configuration Reference [7]**	**Optimum Configuration Present**	**Ω_2 and Ω_3 Present**	**$\Delta\Omega_{23}$ Present**
4	$[90/0]_s$	$[90/0]_s$	$\Omega_2 = 112.78$ $\Omega_3 = 201.66$	$\Delta\Omega_{23} = 88.88$
8	$[0/90/45/0]_s$	$[90/45_2/0]_s$	$\Omega_2 = 118.08$ $\Omega_3 = 207.24$	$\Delta\Omega_{23} = 89.16$ (For $[0/90/45/0]s$ $\Delta\Omega_{23} = 88.68$)
12	$[0_3/90/0_2]_s$	$[0_3/90/0_2]_s$	$\Omega_2 = 112.78$ $\Omega_3 = 207.73$	$\Delta\Omega_{23} = 94.95$
16	$[0_2/90/0/90/0_3]_s$	$[0_2/90/0/90/0_3]_s$	$\Omega_2 = 112.78$ $\Omega_3 = 208.57$	$\Delta\Omega_{23} = 95.79$

The results are in agreement except in a few cases. This may be because Adali and Verijenko [7] neglected the bending-twisting effects for simplicity and imposed special constraints on bending stiffness terms to avoid excessive error. These constraints were

$$D_{16}\,(D_{11}^{\,3}\,D_{22})^{-1/4} \le 0.2 \quad , \quad D_{26}\,(D_{11}\,D_{22}^{\,3})^{-1/4} \le 0.2 \qquad (6.1)$$

In this study, bending-twisting effects are not neglected so these constraints are not used. Since they used enumeration as optimization method, the discrepancy may not be attributed to differences in the methods. By trying all possible configurations, the globally optimal design can be certainly obtained but at the expense of excessive computational times.

6.3. Results for Different Design Domains

When the number of design variables or the range of values that they may take is increased the design space gets larger, i.e. the number of configurations that the search algorithm may try increases. It is very likely that the enlarged design domain may include a better design. Then by choosing a larger design domain, one may obtain improvement in the optimal design. However, existence of a larger number of local optimums in a larger domain causes difficulties in locating the globally optimum configuration. This requires use of a reliable global search algorithm like SA.

In order to see the possible improvements in this respect, the number of distinct fiber angles and the range of values they may take were increased. Frequency separation problem for a 16-ply laminate with an aspect ratio 1.2 was considered. Material properties given in Table 4.1 were used for the laminate. Firstly, a laminate configuration with two distinct lamina angles, $[\alpha_4 / \beta_4]_S$, was optimized. This was a symmetric laminate with four laminae each made of a stack of four plies. Table 6.9 presents the results for different angle increments. An angle increment of 5° means that the possible fiber angles are -90°, -85°,. …, -5°, 0°, 5°,…, 85°, 90°. The results indicate that when the angle increment is decreased, i.e. the range of values that the design variables may take is increased, a better optimal design with a larger frequency separation is obtained.

Table 6.9. Optimum angles of frequency separation problem for different discrete angle increments having $[\alpha_4 / \beta_4]_S$ configuration

Angle Increment	**Optimum Configuration** $[\alpha_4 / \beta_4]_S$	**Frequency Parameter 1. Mode**	**Frequency Parameter 2. Mode**	**Frequency Parameter Difference**
90°	$[0_4/90_4]_S$	49.16	111.71	62.55
45°	$[0_4/90_4]_S$	49.16	111.71	62.55
30°	$[30_4/-60_4]_S$	58.56	125.55	66.99
30°	$[30_4/-60_4]_S$	58.56	125.55	66.99
10°	$[20_4/-80_4]_S$	53.20	120.33	67.13
5°	$[25_4/-70_4]_S$	55.96	123.63	67.67
1°	$[25_4/-72_4]_S$	55.73	123.44	67.71

Then, laminates with four and eight distinct lamina angles ($[\alpha_2 / \beta_2 / \gamma_2 / \theta_2]_S$ and $[\alpha / \beta / \gamma / \theta / \xi / \tau / \varphi / \psi]_S$) were considered. Tables 6.10 and 6.11 show the optimum designs. Since stacking sequence is important for out-of-plane deformation, only the adjacent plies are shown by a single symbol, e.g. $[90/90/90/0/0/0/90/0]_s$ is shown as $[90_3/0_3/90/0]_s$ not as $[90_4/0_4]_s$, because they have different out-of-plane natural frequency.

As seen in the tables, with increasing number of design variables, i.e. number of lamina angles, a larger separation in frequency is obtained. Increasing the number from

two to four resulted in an improvement of about 35 per cent to 45 per cent. With eight distinct angles, a large frequency separation can be obtained even with a limited number of values for angles like {-90º, 0º, 90º}.

Table 6.10. Optimum angles of frequency separation problem for different discrete angle increments having $[\alpha_2 / \beta_2 / \gamma_2 / \theta_2]_s$ configuration

Angle Increment	**Optimum Configuration** $[\alpha_2 / \beta_2 / \gamma_2 / \theta_2]_s$	**Frequency Parameter 1. Mode**	**Frequency Parameter 2. Mode**	**Frequency Parameter Difference**
90°	$[90_2/0_6]_s$	55.67	122.54	66.87
45°	$[0_2/90_2/0_2/-45_2]_s$	52.09	142.74	90.65
30°	$[0_2/90_2/0_2/-30_2]_s$	51.97	142.66	90.69
15°	$[0_2/90_2/0_2/-30_2]_s$	51.97	142.66	90.69
10°	$[0_2/90_2/0_2/-30_2]_s$	51.97	142.66	90.69
5°	$[0_2/90_2/5_2/-35_2]_s$	52.09	143.08	90.99
1°	$[0_2/-88_2/3_2/37_2]_s$	52.09	143.13	91.04

Table 6.11. Optimum angles of frequency separation problem for different discrete angle increments having $[\alpha/\beta/\gamma/\theta/\xi/\tau/\varphi/\psi]_S$ configuration

Angle Increment	**Optimum Configuration** $[\alpha/\beta/\gamma/\theta/\xi/\tau/\varphi/\psi]_S$	**Frequency Parameter 1. Mode**	**Frequency Parameter 2. Mode**	**Frequency Parameter Difference**
90°	$[0/90/0_3/90_3]_s$	51.78	142.88	91.10
45°	$[0/90/0_3/90_3]_s$	51.78	142.88	91.10
30°	$[0/90/0_3/90_3]_s$	51.78	142.88	91.10
15°	$[0/90/0_3/90_3]_s$	51.78	142.88	91.10
10°	$[0/90/0_3/90_3]_s$	51.78	142.88	91.10
5°	$[0/90/0_3/90_3]_s$	51.78	142.88	91.10
1°	$[-2/90/2/0/2/87/89/-85]_s$	51.85	142.97	91.12

6.4. Results for Natural Frequency Maximization and Frequency Separation Maximization

The laminate configuration $[\alpha/\beta/\gamma/\theta]_S$ was optimized to obtain the maximum fundamental frequency. Eight distinct fiber angles were chosen as design variables. The material properties of AS/3501 graphite-epoxy given in Table 4.1 were used in the frequency analysis. Results were obtained for different angle increments. Tables 6.12-6.14 give the results for natural frequency maximization and Tables 6.15-6.16 give the results

for frequency separation maximization. Optimum configuration in Table 6.13 for aspect ratio = 2 is the same with Narita [10] where the frequency parameter is 159.9.

It is observed that better designs with a larger fundamental frequency and a larger frequency separation are obtained when the angle increment is decreased. It is also observed that highly different optimal designs are obtained when the geometry of the plate i.e. its aspect ratio is changed.

Table 6.12. Optimum angles for 8-ply laminate with different aspect ratios for 15° discrete angle increment

a / b	**Optimum Configuration (15° angle increment)**	**Frequency Parameter**
1.0	$[-45/45_3]_S$	56.33
1.2	$[-45/45_3]_S$	68.30
1.3	$[-60/60_3]_S$	75.95
1.5	$[-60/60_3]_S$	93.61
1.7	$[90_4]_S$	116.98
2.0	$[90_4]_S$	159.89

Table 6.13. Optimum angles for 8 ply laminate with different aspect ratios for 5° discrete angle increment

a / b	**Optimum Configuration (5° angle increment)**	**Frequency Parameter**
1.0	$[-45/45_3]_S$	56.33
1.2	$[-50/50_3]_S$	68.88
1.3	$[-55/55_3]_S$	76.27
1.5	$[-65/60/65/60]_S$	93.84
1.7	$[90_4]_S$	116.98
2.0	$[90_4]_S$	159.89

Table 6.14. Optimum angles for 8 ply laminate with different aspect ratios for 1° discrete angle increment

a / b	**Optimum Configuration (1° angle increment)**	**Frequency Parameter**
1.0	$[-45/45_3]_S$	56.33
1.2	$[-52/51_3]_S$	68.91
1.3	$[-56/54_3]_S$	76.28
1.5	$[-67/63_3]_S$	93.89
1.7	$[90_4]_S$	116.98
2.0	$[90_4]_S$	159.89

Table 6.15. Optimum angles for first and second mode frequency separation for 8 ply laminate with different aspect ratios

a / b	**Optimum Configuration (15° angle increment)**	**Frequency Parameter 1. Mode**	**Frequency Parameter 2. Mode**	**Frequency Parameter Difference**
1.0	$[90/0_3]_S$	44.31	115.75	71.44
1.2	$[0/90/0/-30]_S$	51.97	142.67	90.70
1.3	$[15/-60/15_2]_S$	61.87	155.38	93.51
1.5	$[0_2/90/-75]_S$	59.42	160.93	101.51
1.7	$[-15/30/-15/30]_S$	75.10	182.36	107.26
2.0	$[0_4]_S$	67.23	177.23	110.00

Table 6.16. Optimum angles for second and third mode frequency separation for 8 ply laminate with different aspect ratios

a / b	**Optimum Configuration (15° angle increment)**	**Frequency Parameter 2. Mode**	**Frequency Parameter 3. Mode**	**Frequency Parameter Difference**
1.0	$[0_2/75/0]_S$	81.73	153.18	71.45
1.2	$[90/30/-60/90]_S$	113.32	201.58	88.26
1.3	$[90/0/90/15]_S$	118.67	227.13	108.46
1.5	$[-75/0/15_2]_S$	142.32	265.29	122.97
1.7	$[0/90/75/0]_S$	158.32	302.42	144.10
2.0	$[0/75/-15/0]_S$	180.93	335.24	154.31

7. CONCLUSIONS AND FUTURE RESEARCH

In this study, frequency response of symmetric laminated plates was optimized. In order to calculate natural frequency, an analytic method accounting for the effects of bending-twisting coupling was used. For this reason, there was no need to impose limitations on the values of fiber orientation angles or on the stacking sequence. Imposing restrictions on stacking sequence or the possible angle values results in worse optimum designs. Because of the existence of numerous local optimums, a reliable global search algorithm, direct simulated annealing, was used. Discrete fiber angles were taken as design variables. Firstly, a convergence analysis was carried out in order to determine the number of Fourier series terms sufficient to obtain an acceptable accuracy, because the accuracy of the calculated values of frequency was observed to have a significant effect on the optimization results. After ensuring accurate prediction of the mechanical behavior of the laminate, comparisons were made between the results obtained using the present optimization procedure and the results obtained in previous studies for the fundamental frequency maximization and adjacent frequency separation problems. The results were observed to be usually in agreement. Some discrepancies observed in the results may only be attributed to the negligence of bending-twisting coupling in these studies. Therefore, negligence of this effect cannot be justified. Then, the optimum results were obtained for rectangular graphite/epoxy laminates having different aspect ratios with simply-supported edges using different design domains. By increasing the number of distinct lamina angles and the range of values they may take, one may obtain a larger design domain, i.e. more lay-up configurations become possible. In this study, up to eight distinct fiber angles with 1° angle increments were used as design variables to optimize the laminate. Optimization with such a large solution domain was not attempted in previous studies. With a larger domain, it was possible to obtain a better optimum design. Optimization process was repeated for different aspect ratios and for various numbers of distinct fiber angles with different angle increments in order to determine the effect of geometry on the optimum frequency. The optimum configurations were observed to strongly depend on the plate aspect ratio. DSA algorithm yielded consistent and reliable result in all these optimization runs.

In this study, optimum results were found for the symmetric laminates and considering the laminate is thin, transverse shear effects were neglected. For the future study, these limitations may be relaxed and optimum results may be obtained for more general laminate configurations.

APPENDIX A: ANALYSIS OF LAMINATED PLATES UNDER SMALL DEFLECTIONS

The classical lamination theory is applied to derive constitutive equations of the plate. The theory is based on some simplifications in order to reduce a complicated three-dimensional problem to a simple two-dimensional problem. The problem of determining the deformation of a solid body reduces to the deformation of a surface through the use of the Kirchhoff's hypothesis. Then from the 2D model, stress and deformation states can be found.

Restrictions:

- The laminated plate is constructed of orthoropic layers bonded together.
- Each layer is linear elastic.
- There are no body forces.
- Plate thickness is small compared to its length and width.

Assumptions:

- Displacements u, v and w are small in comparison to the plate thickness.
- Kirchhoff hypothesis: a line originally straight and perpendicular to the middle surface of the plate is assumed to remain straight and perpendicular to the middle surface when the laminate is bent. It is equivalent to ignoring out-of-plane shearing strains, that is $\gamma_{xz} = \gamma_{yz} = 0$ where z is the direction perpendicular to the middle surface. In addition, the normal lines are presumed to not to undergo any change in length so that the strain perpendicular to the middle surface is ignored as well, that is $\varepsilon_{zz} = 0$.
- Strains $\varepsilon_{x,}$ ε_{y} and γ_{xy} are small compared to unity.
- Rotatory inertia terms are negligible.

According to the classical lamination theory, the strain-displacement relations are obtained as

$$\begin{bmatrix} \varepsilon_x \\ \varepsilon_y \\ \gamma_{xy} \end{bmatrix} = \begin{bmatrix} \varepsilon_x{}^0 \\ \varepsilon_y{}^0 \\ \gamma_{xy}{}^0 \end{bmatrix} + z \begin{bmatrix} \kappa_x \\ \kappa_y \\ \kappa_{xy} \end{bmatrix} \tag{A.1}$$

where the middle-surface strains are defined as

$$\begin{bmatrix} \varepsilon_x{}^0 \\ \varepsilon_y{}^0 \\ \gamma_{xy}{}^0 \end{bmatrix} = \begin{bmatrix} \dfrac{\partial u^0}{\partial x} \\ \dfrac{\partial v^0}{\partial y} \\ \dfrac{\partial u^0}{\partial y} + \dfrac{\partial v^0}{\partial x} \end{bmatrix} \tag{A.2}$$

and the middle-surface curvatures are defined as

$$\begin{bmatrix} \kappa_x \\ \kappa_y \\ \kappa_{xy} \end{bmatrix} = - \begin{bmatrix} \dfrac{\partial^2 w}{\partial x^2} \\ \dfrac{\partial^2 w}{\partial y^2} \\ 2\dfrac{\partial^2 w}{\partial x \partial y} \end{bmatrix} \tag{A.3}$$

In this study, material and thickness of the plies were assumed to be the same. In the This study concerns only with small amplitude out-of-plane oscillations of laminated plates. Figure A.1 shows a differential element of a plate on which a distributed transverse load $q(x)$ is applied.

In-Plane Forces:

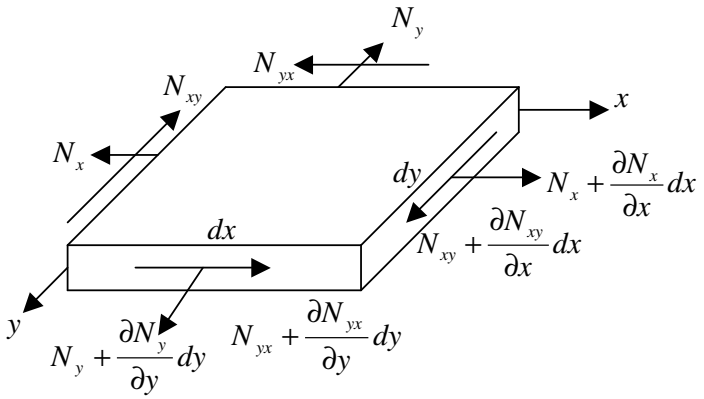

+ Shear Forces:

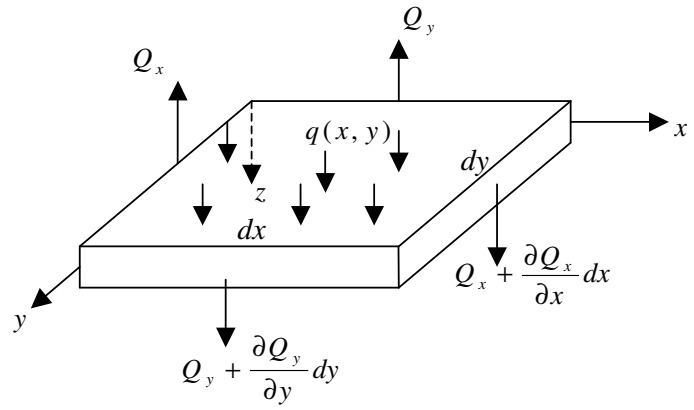

+ Moments:

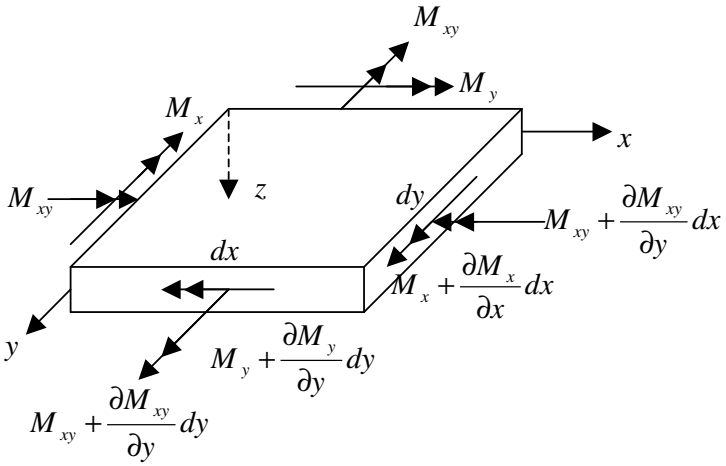

Figure A.1. Stress resultants acting on the laminate

The resultant forces and moments acting on a laminate are obtained by integration of stresses in each layer or lamina through the thickness. N_x, N_y, N_{xy} are in-plane force resultants per unit width. They are defined as the following:

$$N_x = \int_{-h/2}^{h/2} \sigma_x \, dz \tag{A.4}$$

$$N_y = \int_{-h/2}^{h/2} \sigma_y \, dz \tag{A.5}$$

$$N_{xy} = \int_{-h/2}^{h/2} \tau_{xy} \, dz \tag{A.6}$$

Q_x, Q_y are shear force resultants per unit width. They are defined as the following.

$$Q_x = \int_{-h/2}^{h/2} \tau_{xz} \, dz \tag{A.7}$$

$$Q_y = \int_{-h/2}^{h/2} \tau_{yz} \, dz \tag{A.8}$$

M_x, M_y, M_{xy} are moment resultants per unit width. They are defined as the following.

$$M_x = \int_{-h/2}^{h/2} \sigma_x z dz \tag{A.9}$$

$$M_y = \int_{-h/2}^{h/2} \sigma_y z dz \tag{A.10}$$

$$M_{xy} = \int_{-h/2}^{h/2} \tau_{xy} z dz \tag{A.11}$$

All of these forces act simultaneously on the plate. For simplicity they are drawn separately. Newton's Second Law of Motion in the z direction is written as the following:

$$\sum F_z = m\frac{\partial^2 w}{\partial t^2} \tag{A.12}$$

where $\frac{\partial^2 w}{\partial t^2}$ is the acceleration in z direction. Eq. (A.12) can be written as the following:

$$\left(Q_x + \frac{\partial Q_x}{\partial x}dx\right)dy - Q_x dy + \left(Q_y + \frac{\partial Q_y}{\partial y}dy\right)dx - Q_y dx + q dx dy = -\overline{\rho}\frac{\partial^2 w}{\partial t^2}dx\,dy \tag{A.13}$$

$\overline{\rho}$ denotes the mass density per unit area given by

$$\overline{\rho} = \sum_{k=1}^{N} \int_{z^{k-1}}^{z^k} \rho_0 \, dz \tag{A.14}$$

where ρ_0 denotes mass density per unit volume. Because each layer has the same density, it can be taken out of the integral as

$$\overline{\rho} = \rho_0 h \tag{A.15}$$

where h denotes the height of the laminate. Substituting Eq. (A.15) into the Eq. (A.13) and simplifying the Eq. (A.13) yields the following:

$$\frac{\partial Q_x}{\partial x} + \frac{\partial Q_y}{\partial y} + q = -\rho_0 h \frac{\partial^2 w}{\partial t^2} \tag{A.16}$$

Taking moments about x-axis yields

$$\sum M_x = I_x \frac{\partial^3 w}{\partial y \partial t^2} \tag{A.17}$$

where I_x is rotatory inertia with respect to x-axis. Expanding Eq. (A.17) yields the following:

$$\begin{aligned} &-M_y dx - \frac{\partial M_y}{\partial y} dxdy - M_{xy} dy - \frac{\partial M_{xy}}{\partial x} dxdy + Q_y dxdy \\ &+ \frac{\partial Q_y}{\partial y} dxdydy + q(x,y)dxdy\frac{dy}{2} + Q_x dy\frac{dy}{2} \\ &+ \frac{\partial Q_x}{\partial x} dxdy\frac{dy}{2} + M_y dx + M_{xy} dy - Q_x dy\frac{dy}{2} = I_x \frac{\partial^3 w}{\partial y \partial t^2} \end{aligned} \tag{A.18}$$

Neglecting the third-order differentials, Eq. (A.18) is simplified as

$$Q_y - \frac{\partial M_y}{\partial y} - \frac{\partial M_{xy}}{\partial x} = I_x \frac{\partial^3 w}{\partial y \partial t^2} \tag{A.19}$$

Taking moments about y-axis yields

$$\sum M_y = I_y \frac{\partial^3 w}{\partial y \partial t^2} \tag{A.20}$$

where I_y is rotatory inertia with respect to y-axis. Expanding Eq. (A.20) yields the following:

$$\begin{aligned} &M_x dy + \frac{\partial M_x}{\partial x} dxdy + M_{xy} dx + \frac{\partial M_{xy}}{\partial y} dxdy - M_{xy} dx \\ &- M_x dy - Q_x dxdy - \frac{\partial Q_x}{\partial x} dxdydy - q(x,y)dxdy\frac{dy}{2} \\ &- Q_y dx\frac{dy}{2} - \frac{\partial Q_y}{\partial y} dxdy\frac{dy}{2} + Q_y dx\frac{dy}{2} = I_y \frac{\partial^3 w}{\partial y \partial t^2} \end{aligned} \tag{A.21}$$

Neglecting the third-order differentials, Equation (A.18) is simplified as

$$Q_x - \frac{\partial M_x}{\partial x} - \frac{\partial M_{xy}}{\partial y} = I_y \frac{\partial^3 w}{\partial x \partial t^2} \tag{A.22}$$

Substituting Eq. (A.19) and Eq. (A.22) into Eq. (A.16) yields

$$\frac{\partial^2 M_x}{\partial x^2} + 2\frac{\partial^2 M_{xy}}{\partial x \partial y} + \frac{\partial^2 M_y}{\partial y^2} = -q(x,y) - \rho_0 h \frac{\partial^2 w}{\partial t^2} - I_x \frac{\partial^3 w}{\partial y^2 \partial t^2} - I_y \frac{\partial^3 w}{\partial x^2 \partial t^2} \tag{A.23}$$

Neglecting the inertia terms $\left(I_x \frac{\partial^3 w}{\partial y^2 \partial t^2} + I_y \frac{\partial^3 w}{\partial x^2 \partial t^2} \right)$ and setting the transverse load q to zero because of free vibration, Eq. (A.23) yields the following:

$$\frac{\partial^2 M_x}{\partial x^2} + 2\frac{\partial^2 M_{xy}}{\partial x \partial y} + \frac{\partial^2 M_y}{\partial y^2} = -\rho_0 h \frac{\partial^2 w}{\partial t^2} \tag{A.24}$$

Substituting Eqs. (3.1), (A.2) and (A.3) into Eq. (A.24) yields the following.

$$\begin{aligned} &D_{11}\frac{\partial^4 w}{\partial x^4} + 4D_{16}\frac{\partial^4 w}{\partial x^3 \partial y} + 2(D_{12}+2D_{66})\frac{\partial^4 w}{\partial x^2 \partial y^2} + 4D_{26}\frac{\partial^4 w}{\partial x \partial y^3} + D_{22}\frac{\partial^4 w}{\partial y^4} \\ &- B_{11}\frac{\partial^3 u^0}{\partial x^3} - 3B_{16}\frac{\partial^3 u^0}{\partial x^2 \partial y} - (B_{12}+B_{66})\frac{\partial^3 u^0}{\partial x \partial y^2} - B_{26}\frac{\partial^3 u^0}{\partial y^3} - B_{16}\frac{\partial^3 v^0}{\partial x^3} \\ &- (B_{12}+2B_{66})\frac{\partial^3 v^0}{\partial x^2 \partial y} - 3B_{26}\frac{\partial^3 v^0}{\partial x \partial y^2} - B_{22}\frac{\partial^3 v^0}{\partial y^3} = -\rho_0 h \frac{\partial^2 w}{\partial t^2} \end{aligned} \tag{A.25}$$

APPENDIX B: BOUNDARY - CONTINOUS FOURIER SERIES FOR THE SOLUTION OF NATURAL FREQUENCY PROBLEM IN LAMINATED RECTANGULAR PLATES

General solution can be assumed in the following product form because the free vibration motion of the laminate is harmonic in time.

$$w(x, y, t) = e^{i\omega t} V(x, y) \tag{B.1}$$

where i is imaginary unit, ω is angular frequency in radian per second, t is time. $V(x,y)$ is expressed as the following form of double Fourier series.

$$V(x, y) = \sum_{r=1}^{\infty} \sum_{s=1}^{\infty} V_{rs} \sin(\alpha_r x) \sin(\beta_s y) \tag{B.2}$$

$$0 < x < a, \quad 0 < y < b;$$

where

$$\alpha_r = \frac{r\pi}{a}, \quad \beta_s = \frac{s\pi}{b} \tag{B.3}$$

where V_{rs} is plate Fourier coefficients. Multiplying each side of Eq. (B.2) by $(\sin(\alpha_r x)\sin(\beta_s y))$ and taking double integral of each side yields

$$\int_{-a}^{a}\int_{-b}^{b} V(x, y)\sin(\alpha_r x)\sin(\beta_s y)\,dx\,dy = V_{rs}\int_{-a}^{a}\sin(\alpha_r x)\sin(\alpha_r x)\,dx\int_{-b}^{b}\sin(\beta_s y)\sin(\beta_s y)\,dy \tag{B.4}$$

Taking the integrals of the right hand side of the Eq. (B.4) yields

$$V_{rs} = \frac{1}{ab}\int_{-a}^{a}\int_{-b}^{b} V(x, y)\sin(\alpha_r x)\sin(\beta_s y)\,dx\,dy \qquad \text{for r, s} = 1,2,\ldots, \infty \tag{B.5}$$

Taking the first partial derivative of Eq. (B.2) with respect to x yields the following:

$$\frac{\partial V(x,y)}{\partial x} = \sum_{r=0}^{\infty}\sum_{s=1}^{\infty} Y_{rs}\cos(\alpha_r x)\sin(\beta_s y) \tag{B.6}$$

By arranging the right-hand side of the Eq. (B.6) yields

$$\frac{\partial V(x,y)}{\partial x} = \sum_{s=1}^{\infty} Y_{0s}\sin(\beta_s y)dy + \sum_{r=1}^{\infty}\sum_{s=1}^{\infty} Y_{rs}\cos(\alpha_r x)\sin(\beta_s y) \tag{B.7}$$

Multiplying each side of Eq. (B.7) by $(\cos(\alpha_r x)\sin(\beta_s y))$ and taking double integral of each side yields

$$Y_{rs} = \frac{1}{ab}\int_{-a}^{a}\int_{-b}^{b}\frac{\partial V(x,y)}{\partial x}\cos(\alpha_r x)\sin(\beta_s y)dxdy \quad \text{for r, s = 1,2,…, } \infty \tag{B.8}$$

Multiplying each side of Eq. (B.7) by $(\sin(\beta_s y))$ and taking double integral of each side of yields

$$Y_{0s} = \frac{1}{2ab}\int_{-a}^{a}\int_{-b}^{b}\frac{\partial V(x,y)}{\partial x}\sin(\beta_s y)\,dxdy \quad \text{for s = 1,2,…, } \infty \tag{B.9}$$

Taking the first partial derivative of Eq. (B.2) with respect to *y* yields the following:

$$\frac{\partial V(x,y)}{\partial y} = \sum_{r=1}^{\infty}\sum_{s=0}^{\infty} Z_{rs}\sin(\alpha_r x)\sin(\beta_s y) \tag{B.10}$$

Following the same procedure, Eqs. (B.11) and (B.12) are obtained.

$$Z_{rs} = \frac{1}{ab}\int_{-a}^{a}\int_{-b}^{b}\frac{\partial V(x,y)}{\partial y}\sin(\alpha_r x)\cos(\beta_s y)\,dx\,dy \quad \text{for r, s = 1,2,…, } \infty \tag{B.11}$$

$$Z_{0s} = \frac{1}{2ab}\int_{-a}^{a}\int_{-b}^{b}\frac{\partial V(x,y)}{\partial y}\sin(\alpha_r y)\,dx\,dy \quad \text{for r = 1,2,…, } \infty \tag{B.12}$$

If both right-hand and left-hand limits of a function exists but have different values from each other and the value of the function equals to one of them at a point than that point is said to be jump discontinuity and the functions having finite number of jump discontinuities are called piecewise continuous. If a convergent Fourier series (or double Fourier series) is differentiated, the obtained series are not usually convergent. Hobson [30] states that if a function represents a Fourier series which is bounded and piecewise continuous, than the partial derivatives of that function are assumed to be Lebesgue integrable in the domain (-*a*, *a*) × (-*b*, *b*) and shows the following integrals where α is the finite number of jump discontinuity points of f(x) in the domain (-π, π).

$$\int_{-\pi}^{\pi} f(x)\sin(nx)dx = \frac{-1}{n}\left[\begin{array}{l}(-1)^n\{f(\pi-0)-f(-\pi+0)\}\\+\sum\{f(\alpha-0)+f(\alpha+0)\}\cos(n\alpha)\end{array}\right] + \frac{1}{n}\int_{-\pi}^{\pi} f'(x)\cos(nx)dx \tag{B.13}$$

$$\int_{-\pi}^{\pi} f'(x)dx = \{f(\pi-0)-f(-\pi+0)\}+\sum\{f(\alpha-0)+f(\alpha+0)\} \tag{B.14}$$

Because $V(x, y)$ is an odd function with respect to both *x* and *y*, it can be written as the following:

$$V(-x, y) = -V(x, y)\,; \qquad V(x,-y) = -V(x, y) \tag{B.15}$$

Integration by parts is stated as:

$$\int\left(u\frac{dv}{dx}\right)dx = \int\left(\frac{d}{dx}(uv)\right)dx - \int\left(v\frac{du}{dx}\right)dx \tag{B.16}$$

Considering the Eq. (B.8), integration by parts is done as the following:

$$\int_{-a}^{a} \cos(\alpha_r x)\frac{\partial V(x,y)}{\partial x}\,dx = \int_{-a}^{a}\frac{\partial}{\partial x}(V(x,y)\cos(\alpha_r x))\,dx - \int_{-a}^{a} V(x,y)\frac{d}{dx}(\cos(\alpha_r x))\,dx \tag{B.17}$$

Taking the derivatives of right-hand side of the Eq. (B.17) yields

$$\int_{-a}^{a} \frac{\partial V(x,y)}{\partial x}\cos(\alpha_r x)\,dx = \int_{-a}^{a}\left[\frac{\partial V(x,y)}{\partial x}\cos(\alpha_r x) - \alpha_r V(x,y)\sin(\alpha_r x)\right]dx + \int_{-a}^{a}\alpha_r V(x,y)\sin(\alpha_r x)\,dx \tag{B.18}$$

Integration by parts of the integral ($\int_{-a}^{a}\alpha_r V(x,y)\sin(\alpha_r x)\,dx$) in the presence of jump discontinuities yields the following:

$$\int_{-a}^{a}\frac{\partial V(x,y)}{\partial x}\cos(\alpha_r x)dx = \left[\begin{array}{l}(-1)^r\{V(a-0,y)-V(-a+0,y)\} \\ +\sum_{d=1}^{d(Nx)}\{V(x_d-0,y)-V(x_d+0,y)\}\cos(\alpha_r x_d)\end{array}\right] + \alpha_r\int_{-a}^{a}V(x,y)\sin(\alpha_r x)dx \tag{B.19}$$

The summation $\sum$ means to the finite number of points x_d of jump discontinuity of V(x, y) in the interior of (-*a*, *a*). Discontinuities are chosen in the normal direction to the selected edge because if the function vanishes at that edge, different from tangential derivative, normal derivative is not vanish at that edge. Detailed information is provided in Chaudhuri [18].

Multiplying each side of the Eq. (B.19) by ($\frac{1}{ab}\sin(\beta_s y)$) and taking integral yields

$$\frac{1}{ab}\int_{-a}^{a}\int_{-b}^{b}\frac{\partial V(x,y)}{\partial x}\cos(\alpha_r x)\sin(\beta_s y)\,dxdy = \alpha_r \frac{1}{ab}\int_{-a}^{a}\int_{-b}^{b} V(x,y)\sin(\alpha_r x)\sin(\beta_s y)\,dxdy + \frac{1}{ab}\int_{-b}^{b}\{V(a-0,y)-V(-a+0,y)\}(-1)^r \sin(\beta_s y)dy + \frac{1}{ab}\int_{-b}^{b}\sum_{d=1}^{d(Nx)}\{V(x_d-0,y)-V(x_d+0,y)\}\cos(\alpha_r x_d)\sin(\beta_s y)dy \quad \text{(B.20)}$$

Substituting Eqs. (B.5) and (B.8) into the Eq. (B.20) yields

$$Y_{rs} = \alpha_r V_{rs} + \frac{1}{ab}\int_{-b}^{b}\{V(a-0,y)-V(-a+0,y)\}(-1)^r \sin(\beta_s y)dy + \frac{1}{ab}\int_{-b}^{b}\sum_{d=1}^{d(Nx)}\{V(x_d-0,y)-V(x_d+0,y)\}\cos(\alpha_r x_d)\sin(\beta_s y)dy \quad \text{for r, s= 1,2,..}\infty \quad \text{(B.21)}$$

Considering the Eq. (B.9) with the presence of discontinuities yields

$$Y_{0s} = \frac{1}{2ab}\int_{-b}^{b}\{V(a-0,y)-V(-a+0,y)\}\sin(\beta_n y)dy + \frac{1}{2ab}\int_{-b}^{b}\sum_{d=1}^{d(Nx)}\{V(x_d-0,y)-V(x_d+0,y)\}\sin(\beta_s y)dy \quad \text{for r = 1,…, } \infty \quad \text{(B.22)}$$

Considering the Eqs. (B.5) and (B.11) with the presence of discontinuities and following the previous integration by parts procedure yields

$$Z_{rs} = \beta_r V_{rs} + \frac{1}{ab}\int_{-a}^{a}\{V(x,b-0)-V(x,-b+0)\}(-1)^s \sin(\alpha_r x)dx + \frac{1}{ab}\int_{-a}^{a}\sum_{d=1}^{d(Ny)}\{V(x,y_d)-V(x,y_d+0)\}\cos(\beta_s y_d)\sin(\alpha_r x)dx \quad \text{for r,s= 1,2,..}\infty \quad \text{(B.23)}$$

Considering the Eq. (B.12) with the presence of discontinuities yields

$$Z_{r0} = \frac{1}{2ab}\int_{-a}^{a}\{V(x,b-0)-V(x,-b+0)\}\sin(\alpha_m x)dx + \frac{1}{2ab}\int_{-a}^{a}\sum_{d=1}^{d(Ny)}\{V(x,y_d-0)-V(x,y_d+0)\}\sin(\alpha_m x)dx \quad \text{for r, s= 1,2,..}\infty \quad \text{(B.24)}$$

V(x, y) is an odd function of both *x* and *y* and it is continuous in the domain (0, *a*) × (0, *b*) and does not vanish at the edges, x = 0, x = a, and y = 0, y = b, is considered. The half-range double Fourier series V(x,y) and its two first partial derivatives are given below.

$$V_{rs} = \frac{4}{ab}\int_0^a \int_0^b V(x,y)\sin(\alpha_r x)\sin(\beta_s y)dxdy \qquad \text{for r, s = 1,2,…, } \infty \qquad \text{(B.25)}$$

$$Y_{rs} = \frac{4}{ab}\int_0^a \int_0^b \frac{\partial V(x,y)}{\partial x}\cos(\alpha_r x)\sin(\beta_s y)\,dx\,dy \qquad \text{for r, s = 1,2,…, } \infty \qquad \text{(B.26)}$$

$$Y_{0s} = \frac{1}{ab}\int_0^a \int_0^b \frac{\partial V(x,y)}{\partial x}\sin(\beta_s y)\,dx\,dy \qquad \text{for s = 1,2,…, } \infty \qquad \text{(B.27)}$$

$$Z_{rs} = \frac{4}{ab}\int_0^a \int_0^b \frac{\partial V(x,y)}{\partial y}\sin(\alpha_r x)\cos(\beta_s y)\,dx\,dy \qquad \text{for r, s = 1,2,…, } \infty \qquad \text{(B.28)}$$

$$Z_{0s} = \frac{1}{ab}\int_0^a \int_0^b \frac{\partial V(x,y)}{\partial y}\sin(\alpha_r x)\,dx\,dy \qquad \text{for r = 1,2,…, } \infty \qquad \text{(B.29)}$$

The first partial derivatives $\frac{\partial V(x,y)}{\partial x}$ and $\frac{\partial V(x,y)}{\partial y}$ can not be represented by the term by term differentiation of the series given by the Eq. (B.25), because the first partial derivatives $\frac{\partial V(x,y)}{\partial x}$ and $\frac{\partial V(x,y)}{\partial y}$, have jump discontinuities at the lines x = 0, y = 0 and V(x,y) is not an even function as shown in Eq. (B.30).

$$V(a-0,y) \neq V(-a+0,y) \neq 0\,; \qquad V(x,b-0) \neq V(x,-b+0) \neq 0\,; \qquad \text{(B.30)}$$

The Fourier coefficients for $\frac{\partial V(x,y)}{\partial x}$ and $\frac{\partial V(x,y)}{\partial y}$, must be obtained by substituting in Eqs. (B.21– B.24) $d^{(Nx,y)} = 1$; $x_1 = 0$, $y_1 = 0$ and by using the following property which is valid for odd functions given in Eqs. (B.31) and (B.32).

$$V(-a+0,y) = -V(a-0,y)\,; \qquad V(0-0,y) = -V(0+0,y)\,; \qquad \text{(B.31)}$$

$$V(x,-b+0) = -V(x,b-0)\,; \qquad V(x,0-0) = -V(x,0+0) \tag{B.32}$$

Substituting Eq. (B.31) into the Eq. (B.21) and taking the half-range Fourier series yields the following:

$$Y_{rs} = \alpha_r V_{rs} + \frac{4}{ab}\int_0^b \left\{V(a-0,y)\,(-1)^r - V\,(0+0,y)\right\}\sin(\beta_s y)\,dy \tag{B.33}$$

Substituting Eq. (B.31) into the Eq. (B.22) and taking the half-range Fourier series yields the following:

$$Y_{0s} = \frac{2}{ab}\int_0^b \{V(a-0,y) - V(0+0,y)\}\sin(\beta_s y)\,dy \tag{B.34}$$

Substituting Eq. (B.32) into the Eq. (B.23) and taking the half-range Fourier series yields the following:

$$Z_{rs} = \beta_s V_{rs} + \frac{4}{ab}\int_0^a \left\{V(x,b-0)\,(-1)^s - V(x,0+0)\right\}\sin(\alpha_m x)\,dx \tag{B.35}$$

Substituting Eq. (B.32) into the Eq. (B.24) and taking the half-range Fourier series yields the following:

$$Z_{r0} = \frac{2}{ab}\int_0^b \{V(x,b-0) - V(x,0+0)\}\sin(\alpha_r x)\,dx \tag{B.36}$$

a_s, b_s, c_r, d_r, $\bar{a}_s$, $\bar{b}_s$, $\bar{c}_r$, $\bar{d}_r$ are defined in the following Eqs. (B.37- B.44)

$$a_s = \frac{4}{ab}\int_0^b [V(a,y) - V(0,y)]\sin(\beta_s y)dy \tag{B.37}$$

$$b_s = -\frac{4}{ab}\int_0^b [V(a,y) - V(0,y)]\sin(\beta_s y)dy \tag{B.38}$$

$$c_r = \frac{4}{ab}\int_0^a [V(x,b) - V(x,o)]\sin(\alpha_m x)dx \tag{B.39}$$

$$d_r = -\frac{4}{ab}\int_0^a [V(x,b) - V(x,o)]\sin(\alpha_m x)dx \tag{B.40}$$

$$\bar{a}_s = \frac{4}{ab}\int_0^b \left[\frac{\partial^2 V(a,y)}{\partial x^2} - \frac{\partial^2 V(0,y)}{\partial x^2}\right]\sin(\beta_s y)dy \tag{B.41}$$

$$\bar{b}_s = -\frac{4}{ab}\int_0^b \left[\frac{\partial^2 V(a,y)}{\partial x^2} - \frac{\partial^2 V(0,y)}{\partial x^2}\right]\sin(\beta_s y)dy \tag{B.42}$$

$$\bar{c}_r = \frac{4}{ab}\int_0^a \left[\frac{\partial^2 V(x,b)}{\partial y^2} - \frac{\partial^2 V(x,0)}{\partial y^2}\right]\sin(\alpha_m x)dx \tag{B.43}$$

$$\bar{d}_r = -\frac{4}{ab}\int_0^a \left[\frac{\partial^2 V(x,b)}{\partial y^2} - \frac{\partial^2 V(x,0)}{\partial y^2}\right]\sin(\alpha_m x)dx \tag{B.44}$$

Substituting Eq. (B.37) into Eq. (B.34), and substituting the Eqs (B.37) and (B.38) into Eq. (B.33), and together substituting them into Eq. (B.7) yields the following:

$$\frac{\partial V(x,y)}{\partial x} = \frac{1}{2}\sum_{s=1}^{\infty} a_s \sin(\beta_s y) + \sum_{r=1}^{\infty}\sum_{s=1}^{\infty}(\alpha_r V_{rs} + a_s\phi_r + b_s\psi_r)\cos(\alpha_r x)\sin(\beta_s y) \tag{B.45}$$

$$0 \le x \le a, \qquad 0 < y < b;$$

where

$$(\phi_i, \psi_i) = \begin{Bmatrix} (0,1), & i = odd \\ (1,0), & i = even \end{Bmatrix} \tag{B.46}$$

By substituting Eq. (B.39) into Eq. (B.36), and Eqs. (B.39) and (B.40) into Eq. (B.35), and together substituting them into Eq. (B.10) yields the following:

$$\frac{\partial V(x,y)}{\partial y}=\frac{1}{2}\sum_{s=1}^{\infty}c_r\sin(\alpha_r x)+\sum_{r=1}^{\infty}\sum_{s=1}^{\infty}(\beta_s V_{rs}+c_r\phi_s+d_r\psi_s)\sin(\alpha_r x)\cos(\beta_s y) \quad \text{(B.47)}$$

$$0<x<a\,,\qquad 0\le y\le b\,;$$

By following the same procedure, yields the following Eqs. (B.48- B.52):

$$\frac{\partial^2 V(x,y)}{\partial x\partial y}=\frac{\partial^2 V(x,y)}{\partial y\partial x}=\frac{1}{2}\sum_{s=1}^{\infty}\alpha_r c_r\cos(\alpha_r x)+\frac{1}{2}\sum_{s=1}^{\infty}\beta_s a_s\cos(\beta_s y)$$
$$+\sum_{r=1}^{\infty}\sum_{s=1}^{\infty}\{\alpha_r\beta_s V_{rs}+\beta_s(a_s\phi_r+b_s\psi_r)+\alpha_r(c_r\phi_s+d_r\psi_s)\}\cos(\alpha_r x)\cos(\beta_s y) \quad \text{(B.48)}$$

$$0\le x\le a\,,\qquad 0\le y\le b\,;$$

$$\frac{\partial^3 V(x,y)}{\partial x^3}=\frac{1}{2}\sum_{s=1}^{\infty}\bar{a}_s\sin(\beta_s y)$$
$$+\sum_{r=1}^{\infty}\sum_{s=1}^{\infty}\{-\alpha_r{}^2(\alpha_r V_{rs}+a_s\phi_r+b_s\psi_r)+\bar{a}_s\phi_s+\bar{b}_s\psi_s)\}\cos(\alpha_r x)\sin(\beta_s y) \quad \text{(B.49)}$$

$$0\le x\le a\,,\qquad 0<y<b\,;$$

$$\frac{\partial^3 V(x,y)}{\partial y^3}=\frac{1}{2}\sum_{s=1}^{\infty}\bar{c}_r\sin(\alpha_r x)$$
$$+\sum_{r=1}^{\infty}\sum_{s=1}^{\infty}\{-\beta_s{}^2(\beta_s V_{rs}+c_r\phi_s+d_r\psi_s)+\bar{c}_r\phi_s+\bar{d}_r\psi_s)\}\sin(\alpha_r x)\cos(\beta_s y) \quad \text{(B.50)}$$

$$0<x<a\,,\qquad 0\le y\le b\,;$$

$$\frac{\partial^4 V(x,y)}{\partial x^3\partial y}=\frac{\partial^4 V(x,y)}{\partial y\partial x^3}=-\frac{1}{2}\sum_{r=1}^{\infty}\alpha_r{}^3 c_r\cos(\alpha_r x)+\frac{1}{2}\sum_{s=1}^{\infty}\beta_s\bar{a}_s\cos(\beta_s y)$$
$$+\sum_{r=1}^{\infty}\sum_{s=1}^{\infty}\begin{bmatrix}-\alpha_r{}^2\{\alpha_r\beta_s V_{rs}+\beta_s(a_s\phi_r+b_s\psi_r)+\alpha_r(c_r\phi_s+d_r\psi_s)\}\\+\beta_s(\bar{a}_s\phi_r+\bar{b}_s\psi_r)\end{bmatrix}\cos(\alpha_r x)\cos(\beta_s y) \quad \text{(B.51)}$$

$$0\le x\le a\,,\qquad 0\le y\le b\,;$$

$$\frac{\partial^4 V(x,y)}{\partial x\partial y^3}=\frac{\partial^4 V(x,y)}{\partial y^3\partial x}=-\frac{1}{2}\sum_{r=1}^{\infty}\alpha_r\bar{c}_r\cos(\alpha_r x)+\frac{1}{2}\sum_{s=1}^{\infty}\beta_s{}^3 a_s\cos(\beta_s y)$$
$$+\sum_{r=1}^{\infty}\sum_{s=1}^{\infty}\begin{bmatrix}-\beta_s{}^2\{\alpha_r\beta_s V_{rs}+\alpha_r(c_r\phi_s+d_r\psi_s)+\beta_s(a_s\phi_r+b_s\psi_r)\}\\+\alpha_r(\bar{c}_r\phi_s+\bar{d}_r\psi_s)\end{bmatrix}\cos(\alpha_r x)\cos(\beta_s y) \quad \text{(B.52)}$$

$$0 \le x \le a\,, \qquad 0 \le y \le b\,;$$

The remaining derivatives can be obtained by term by term differentiation such as taking partial derivative of Eq. (B.49) with respect to x gives the following:

$$\frac{\partial^4 V(x,y)}{\partial x^4} = \sum_{r=1}^{\infty}\sum_{s=1}^{\infty}\left\{\alpha_r{}^3(\alpha_r V_{rs} + a_s\phi_r + b_s\psi_r) - \alpha_r(\bar{a}_s\phi_s + \bar{b}_s\psi_s)\right\}\sin(\alpha_r x)\sin(\beta_s y) \quad \text{(B.53)}$$

Taking partial derivative of Eq. (B.50) with respect to y gives the following:

$$\frac{\partial^4 V(x,y)}{\partial y^4} = \sum_{r=1}^{\infty}\sum_{s=1}^{\infty}\left\{\beta_s{}^3(\beta_s V_{rs} + c_r\phi_s + d_r\psi_s) - \beta_s(\bar{c}_r\phi_s + \bar{d}_r\psi_s)\right\}\sin(\alpha_r x)\sin(\beta_s y) \quad \text{(B.54)}$$

Taking twice partial derivative of Eq. (B.48) with respect to x and y gives the following:

$$\frac{\partial^2 V(x,y)}{\partial x^2 \partial y^2} = \sum_{r=1}^{\infty}\sum_{s=1}^{\infty}\alpha_r\beta_s\{\alpha_r\beta_s V_{rs} + \beta_s(a_s\phi_r + b_s\psi_r) + \alpha_r(c_r\phi_s + d_r\psi_s)\}\sin(\alpha_r x)\sin(\beta_s y) \quad \text{(B.55)}$$

Taking the double derivative of Eq. (B.1) with respect to time yields the following:

$$\frac{\partial^2 w(x,y,t)}{\partial t^2} = -\omega^2 e^{i\omega t} V(x,y) \quad \text{(B.56)}$$

Substituting Eq. (B.2) into Eq. (B.56) yields

$$\frac{\partial^2 w(x,y,t)}{\partial t^2} = -\omega^2 e^{i\omega t} V_{rs}\sin(\alpha_r x)\sin(\beta_s y) \quad \text{(B.57)}$$

Substituting Eqs. (B.53-B.55) and (B.57) into the governing Eq. (B.58) yields

$$\sum_{r=1}^{\infty}\sum_{s=1}^{\infty}\left[F_1(r,s)\sin(\alpha_r x)\sin(\beta_s y)+F_2(r,s)\cos(\alpha_r x)\cos(\beta_s y)\right] + \sum_{r=1}^{\infty}F_3(r)\cos(\alpha_r x)+\sum_{s=1}^{\infty}F_4(s)\cos(\beta_s y)=0 \tag{B.58}$$

in which

$$\begin{aligned} F_1(r,s) &= D_{11}\left\{\alpha_r{}^3(\alpha_r V_{rs}+a_s\phi_r+b_s\psi_r)-\alpha_r(\bar{a}_s\phi_r+\bar{b}_s\psi_r)\right\} \\ &+ 2(D_{12}+2D_{66})\alpha_r\beta_s\left\{\alpha_r\beta_s V_{rs}+\beta_s(a_s\phi_r+b_s\psi_r)+\alpha_r(c_r\phi_s+d_r\psi_s)\right\} \\ &+ D_{22}\left\{\beta_s{}^3(\beta_s V_{rs}+c_r\phi_s+d_r\psi_s-\beta_s(\bar{c}_r\phi_s+\bar{d}_r\psi_s)\right\}-\bar{\rho}\omega^2 V_{rs} \end{aligned} \tag{B.59}$$

$$\begin{aligned} F_2(r,s) &= 4D_{16}\left[-\alpha_r{}^2\{\alpha_r\beta_s V_{rs}+\beta_s(a_s\phi_r+b_s\psi_r)+\alpha_r(c_r\phi_s+d_r\psi_s)\}+\beta_s(\bar{a}_s\phi_r+\bar{b}_s\psi_r)\right] \\ &+ 4D_{26}\left\{-\beta_s{}^2(\alpha_r\beta_s V_{rs}+\beta_s(a_s\phi_r+b_s\psi_r)+\alpha_r(c_r\phi_s+d_r\psi_s)\right\}+\alpha_r(\bar{c}_r\phi_s+\bar{d}_r\psi_s) \end{aligned} \tag{B.60}$$

$$F_3(r)=2(-D_{16}\alpha_r{}^3 c_r+D_{26}\alpha_r\bar{c}_r) \tag{B.61}$$

$$F_4(s)=2(-D_{26}\beta_s{}^3 a_s+D_{16}\beta_s\bar{a}_s) \tag{B.62}$$

Cosine function can be written in the form of Fourier sine series as shown in Green and Hearmon [21]:

$$\cos(\alpha_r x)=\sum_{m=1}^{\infty}h_{rm}\sin(\alpha_m x);\qquad r\neq 0; \tag{B.63}$$

$$\cos(\beta_s y)=\sum_{m=1}^{\infty}h_{sn}\sin(\beta_n y);\qquad s\neq 0; \tag{B.64}$$

Double cosine function can be written in the form of double sine series:

$$\cos(\alpha_r x)\cos(\beta_s y)=\sum_{m=1}^{\infty}\sum_{n=1}^{\infty}h_{rm}h_{sn}\sin(\alpha_m x)\sin(\beta_n y) \tag{B.65}$$

$$r \neq 0, \qquad s \neq 0; \qquad 0 < x < a; \qquad 0 < y < b;$$

Fourier coefficients can be find in the same manner used in Eqs. (B.4) and (B.5):

$$h_{rm} = \begin{cases} \dfrac{4m}{\pi(m^2 - r^2)}, & \text{m + r = odd;} \\ 0, & \text{m + r = even;} \end{cases} \tag{B.66}$$

$$h_{sn} = \begin{cases} \dfrac{4n}{\pi(n^2 - s^2)}, & \text{n + s = odd;} \\ 0, & \text{n + s = even;} \end{cases} \tag{B.67}$$

Substituting Eqs. (B.66) and (B.67) into Eq. (B.58-B.62) yields the following:

$$\begin{aligned}
&F(r,s)V_{rs} - 4\sum_{m=1}^{\infty}\sum_{n=1}^{\infty}\alpha_m\beta_n(\gamma\alpha_m{}^2 + \chi\beta_n{}^2)h_{rm}h_{sn}V_{mn} \\
&+ 4\gamma\sum_{m=1}^{\infty}\sum_{n=1}^{\infty}\left[-\alpha_m{}^2\{\beta_n(a_n\phi_m + b_n\psi_m) + \alpha_n(c_m\phi_n + d_m\psi_n)\} + \beta_n(\bar{a}_n\phi_m + \bar{b}_n\psi_m)\right]h_{rm}h_{sn} \\
&+ 4\chi\sum_{m=1}^{\infty}\sum_{n=1}^{\infty}\left[-\beta_n{}^2\{\beta_n(a_n\phi_m + b_n\psi_m) + \alpha_m(c_m\phi_n + d_m\psi_n)\} + \alpha_m(\bar{c}_m\phi_n + \bar{d}_m\psi_n)\right]h_{rm}h_{sn} \\
&+ 2\left[\sum_{m=1}^{\infty}\alpha_m(\chi\bar{c}_m - \gamma\alpha_m{}^2c_m)h_{rm} + \sum_{n=1}^{\infty}\beta_n(\gamma\bar{a}_n - \chi\beta_n{}^2a_n)h_{sn}\right] \\
&= -\alpha_r\left\{\alpha_r{}^2(a_s\phi_r + b_s\psi_r) - (\bar{a}_s\phi_r + \bar{b}_s\psi_r)\right\} \\
&\quad - 2\xi\left\{\beta_s(a_s\phi_r + b_s\psi_r) - \alpha_r(c_r\phi_s + d_r\psi_s)\right\} \\
&\quad - \eta\beta_s\left\{\beta_s{}^2(c_r\phi_s + d_r\psi_s) - (\bar{c}_r\phi_s + \bar{d}_r\psi_s)\right\}
\end{aligned} \tag{B.68}$$

where

$$F(r,s) = \alpha_r{}^4 + 2\zeta\alpha_r{}^2\beta_s{}^2 + \eta\beta_s{}^4 - \lambda \tag{B.69}$$

$$\zeta = \frac{(D_{12} + 2D_{66})}{D_{11}} \tag{B.70}$$

$$\eta = \frac{D_{22}}{D_{11}} \tag{B.71}$$

$$\gamma = \frac{D_{16}}{D_{11}} \tag{B.72}$$

$$\chi = \frac{D_{26}}{D_{11}} \tag{B.73}$$

$$\lambda = \frac{\overline{\rho}\omega^2}{D_{11}} \tag{B.74}$$

Boundary conditions for simply supported laminated plate is given in the following:

$$V(0, y) = 0 \tag{B.75}$$

$$D_{11}\frac{\partial^2 V(0,y)}{\partial x^2} + 2D_{16}\frac{\partial^2 V(0,y)}{\partial x \partial y} + D_{12}\frac{\partial^2 V(0,y)}{\partial y^2} = 0 \tag{B.76}$$

$$V(a, y) = 0 \tag{B.77}$$

$$D_{11}\frac{\partial^2 V(a,y)}{\partial x^2} + 2D_{16}\frac{\partial^2 V(a,y)}{\partial x \partial y} + D_{12}\frac{\partial^2 V(a,y)}{\partial y^2} = 0 \tag{B.78}$$

$$V(x, 0) = 0 \tag{B.79}$$

$$D_{12}\frac{\partial^2 V(x,0)}{\partial x^2} + 2D_{26}\frac{\partial^2 V(x,0)}{\partial x \partial y} + D_{22}\frac{\partial^2 V(x,0)}{\partial y^2} = 0 \tag{B.80}$$

$$V(x, b) = 0 \tag{B.81}$$

$$D_{12}\frac{\partial^2 V(x,b)}{\partial x^2}+2D_{26}\frac{\partial^2 V(x,b)}{\partial x\partial y}+D_{22}\frac{\partial^2 V(x,b)}{\partial y^2}=0 \tag{B.82}$$

The assumed solution is given from Eqs. (B.75), (B.77), (B.79) and (B.81) as the following:

$$V(x,y)=\sum_{r=1}^{\infty}\sum_{s=1}^{\infty}V_{rs}\sin(\alpha_r x)\sin(\beta_s y) \tag{B.83}$$
$$0\le x\le a, \qquad 0\le y\le b$$

Substituting Eqs. (B.75) and (B.77) into Eqs. (B.37) and (B.38) yields the following:

$$a_s=0 \text{ and } b_s=0 \tag{B.84}$$

Substituting Eqs (B.79) and (B.81) into Eqs. (B.39) and (B.40) yields the following:

$$c_r=0 \text{ and } d_r=0 \tag{B.85}$$

Vanishing the unknown boundary Fourier coefficients a_s, b_s, c_r, d_r in the Eq. (B.68) yields

$$\begin{aligned}
&F(r,s)V_{rs}-4\sum_{m=1}^{\infty}\sum_{n=1}^{\infty}\alpha_m\beta_n(\gamma\alpha_m{}^2+\chi\beta_n{}^2)h_{mr}h_{sn}V_{mn}\\
&+4\gamma\sum_{n=1}^{\infty}\left\{\frac{1}{2}\beta_n\bar{a}_n h_{sn}+\sum_{m=1}^{\infty}\beta_n(\bar{a}_n\phi_m+\bar{b}_n\psi_m)h_{mr}h_{sn}\right\}\\
&+4\chi\sum_{m=1}^{\infty}\left\{\frac{1}{2}\alpha_m\bar{c}_m h_{rm}+\sum_{n=1}^{\infty}\alpha_m(\bar{c}_m\phi_n+\bar{d}_m\psi_n)h_{mr}h_{sn}\right\}\\
&=\alpha_r(\bar{a}_s\phi_r+\bar{b}_s\psi_r)+\eta\beta_s(\bar{c}_r\phi_s+\bar{d}_r\psi_s)
\end{aligned} \tag{B.86}$$

Green and Hearmon [21] used the following summation result for the simplification of Eq. (B.92):

$$\frac{1}{2n^2} + \sum_{m=2...even}^{\infty} \frac{1}{(n^2 - m^2)} = 0, \qquad n = odd; \tag{B.87}$$

$$\sum_{m=1...odd}^{\infty} \frac{1}{(n^2 - m^2)} = 0, \qquad n = even. \tag{B.88}$$

Equation (B.86) is simplified as the following:

$$\begin{aligned} &F(r,s)V_{rs} - 4\sum_{m=1}^{\infty}\sum_{n=1}^{\infty} \alpha_m \beta_n (\gamma \alpha_m{}^2 + \chi \beta_n{}^2) h_{mr} h_{sn} V_{mn} \\ &= \alpha_r (\bar{a}_s \phi_r + \bar{b}_s \psi_r) + \eta \beta_s (\bar{c}_r \phi_s + \bar{d}_r \psi_s) \end{aligned} \tag{B.89}$$

Equations (B.41) and (B.42) and the definition of Fourier coefficient yields

$$\frac{\partial^2 V(0,y)}{\partial x^2} = \frac{a}{4}\sum_{s=1}^{\infty} (-\bar{a}_s - \bar{b}_s) \sin(\beta_s y) \tag{B.90}$$

$$\frac{\partial^2 V(a,y)}{\partial x^2} = \frac{a}{4}\sum_{s=1}^{\infty} (\bar{a}_s - \bar{b}_s) \sin(\beta_s y) \tag{B.91}$$

Equations (B.43) and (B.44) and the definition of Fourier coefficient yields

$$\frac{\partial^2 V(x,0)}{\partial y^2} = \frac{b}{4}\sum_{r=1}^{\infty} (-\bar{c}_r - \bar{d}_r) \sin(\alpha_r x) \tag{B.92}$$

$$\frac{\partial^2 V(x,b)}{\partial y^2} = \frac{b}{4}\sum_{r=1}^{\infty} (\bar{c}_r - \bar{d}_r) \sin(\alpha_r x) \tag{B.93}$$

Vanishing the unknown boundary Fourier coefficients a_s, b_s, c_r, d_r in Eq. (B.48) yields the following:

$$\frac{\partial^2 V(x,y)}{\partial x \partial y} = \frac{\partial^2 V(x,y)}{\partial y \partial x} = \sum_{r=1}^{\infty}\sum_{s=1}^{\infty} \alpha_r \beta_s V_{rs} \cos(\alpha_r x)\cos(\beta_s y) \qquad (B.94)$$

$$0 \le x \le a, \qquad 0 \le y \le b$$

Substituting Eqs. (B.90) and (B.94) into Eq. (B.76) yields the following:

$$D_{11}\frac{a}{4}\sum_{s=1}^{\infty}(-\bar{a}_s - \bar{b}_s)\sin(\beta_s y) + 2D_{16}\sum_{r=1}^{\infty}\sum_{s=1}^{\infty}\alpha_r \beta_s V_{rs}\cos(\beta_s y) = 0 \qquad (B.95)$$

Substituting Eqs. (B.91) and (B.94) into Eq. (B.78) gives the following:

$$D_{11}\frac{a}{4}\sum_{s=1}^{\infty}(\bar{a}_s - \bar{b}_s)\sin(\beta_s y) + 2D_{16}\sum_{r=1}^{\infty}\sum_{s=1}^{\infty}\alpha_r \beta_s V_{rs}(-1)^r\cos(\beta_s y) = 0 \qquad (B.96)$$

$$\cos(\beta_s y) = \sum_{r=1}^{\infty} h_{sr}\sin(\beta_r y); \qquad s \neq 0; \qquad (B.97)$$

$$h_{sr} = \begin{cases} \dfrac{4r}{\pi(r^2 - s^2)}, & \text{r + s = odd;} \\ 0, & r + \text{s} = \text{even;} \end{cases} \qquad (B.98)$$

Substituting Eq. (B.97) into Eq. (B.95) gives the following:

$$D_{11}\,a\sum_{s=1}^{\infty}(\bar{a}_s + \bar{b}_s) = 8\,D_{16}\sum_{m=1}^{\infty}\sum_{n=1}^{\infty}\alpha_m \beta_n V_{mn} h_{ns} \qquad (B.99)$$

Substituting Eq. (B.97) into Eq. (B.96) gives the following:

$$D_{11}\,a\sum_{s=1}^{\infty}(\bar{a}_s - \bar{b}_s) = -8\,D_{16}\sum_{m=1}^{\infty}\sum_{n=1}^{\infty}(-1)^m \alpha_m \beta_n V_{mn} h_{ns} \qquad (B.100)$$

Equations (B.99) and (B.100) yields the following equations:

$$\overline{a}_s = 8\frac{D_{16}}{D_{11}}\sum_{m=1}^{\infty}\sum_{n=odd}^{\infty}\alpha_m \beta_n V_{mn} h_{ns} \tag{B.101}$$

$$\overline{b}_s = 8\frac{D_{16}}{D_{11}}\sum_{m=1}^{\infty}\sum_{n=even}^{\infty}\alpha_m \beta_n V_{mn} h_{ns} \tag{B.102}$$

Following exactly the same procedure used previously, substituting Eqs. (B.92-B.94) into Eqs. (B.80) and (B.82) yields

$$\overline{c}_r = 8\frac{D_{26}}{D_{22}}\sum_{n=1}^{\infty}\sum_{m=odd}^{\infty}\alpha_m \beta_n V_{mn} h_{mr} \tag{B.103}$$

$$\overline{d}_r = 8\frac{D_{26}}{D_{22}}\sum_{n=1}^{\infty}\sum_{m=even}^{\infty}\alpha_m \beta_n V_{mn} h_{mr} \tag{B.104}$$

Substituting Eqs. (B.101-B.104) and (B.72-B.73) into the Eq. (B.89) yields the following.

$$F(r,s)V_{rs} - 2\sum_{m=1}^{\infty}\sum_{n=1}^{\infty}\alpha_m \beta_n \left\{\gamma(\alpha_m{}^2 + \alpha_r{}^2) + \chi(\beta_s{}^2 + \beta_n{}^2)\right\} h_{rm} h_{sn} V_{mn} = 0 \tag{B.105}$$

REFERENCES

1. Bert, C. W., "Optimal Design of a Composite-Material Plate to Maximize Its Fundamental Frequency", *Journal of Sound and Vibration*, Vol. 50, No. 2, pp. 229-237, 1977.

2. Bert, C. W., "Design of Clamped Composite-Material Plates to Maximize Fundamental Frequency", *Journal of Mechanical Design*, Vol. 100, pp. 274-278, 1978.

3. Reiss, R. and S. Ramachandran, "Maximum Frequency Design of Symmetric Angle-Ply Laminates*", Composite Structures* 4, Vol. 1, in I. H. Marshall (ed.), *Analysis and Design Studies*, pp. 1476-1487, Elsevier, London, 1987.

4. Mateus, H. C., C. M. M. Soares and C. A. M. Soares, "*Sensitivity Analysis and Optimal Design of Thin Laminated Composite Structures*", Computers & Structures, Vol. 41, No. 3, pp. 501-508, 1991.

5. Soares, C. M. M., V. F. Correia and H. Mateus, "A Discrete Model for the Optimal Design of Thin Composite Plate-Shell Type Structures Using a Two-Level Approach", *Composite Structures*, Vol. 30, pp. 147-157, 1995.

6. Rao, S. S. and K. Singh, "Optimum Design Laminates with Natural Frequency Constraints", *Journal of Sound and Vibration*, Vol. 67, No. 1, pp. 101-112, 1979.

7. Adali, S. and V. E. Verijenko, "Optimum Stacking Sequence Design of Symmetric Hybrid Laminates Undergoing Free Vibrations", *Composite Structures*, Vol. 54, pp. 131-138, 2001.

8. Farshi, B. and R Rabiei, "Optimum Design of Composite Laminates for Frequency Constraints", *Composite Structures*, Vol. 81, pp. 587-597, 2007.

9. Duffy, K. J. and S. Adali, “Optimal Fibre Orientation of Antisymmetric Hybrid Laminates for Maximum Fundamental Frequency and Frequency Separation”, *Journal of Sound and Vibration*, Vol. 146, No. 2, pp. 181-190, 1991.

10. Narita, Y., “Layerwise Optimization for the Maximum Fundamental Frequency of Laminated Composite Plates”, *Journal of Sound and Vibration*, Vol. 263, pp. 1005-1016, 2003.

11. Todoroki, A. and T. Ishikawa, “Design of Experiments for Stacking Sequence Optimizations with Genetic Algorithm Using Response Surface Approximation”, *Composite Structures*, Vol. 64, pp. 349-357, 2004.

12. Sivakumar, K., N. G. R. Iyengar and K. Deb, “Optimum Design of Laminated Plates with Cutouts Using a Genetic Algorithm”, *Composite Structures*, Vol. 42, pp. 265-279, 1998.

13. Adams, D. B., L. T. Watson and Z. Gürdal, “Genetic Algorithm Optimization and Blending of Composite Laminates by Locally Reducing Laminate Thickness”, *Advances in Engineering Software*, Vol. 35, pp. 35-43, 2004.

14. Apalak, M. K., M. Yildirim and R. Ekici, “Layer Optimisation for Fundamental Frequency of Laminated Composite Plates for Different Edge Conditions”, *Composites Science and Technology*, Vol. 68, pp. 537-550, 2008.

15. Erdal, O. and F. O. Sönmez, “Optimum Design of Laminates for Maximum Buckling Load Capacity Using Simulated Annealing”, *Composite Structures*, Vol. 71, pp. 45-52, 2005.

16. Moita, J. M. S., V. M. F. Correia and P. G. Martins, “Optimal Design in Vibration Control of Adaptive Structures Using a Simulated Annealing Algorithm”, *Composite Structures*, Vol. 75, pp. 79-87, 2006.

17. Whitney J. M. and A. W. Leissa, “Analysis of Heterogeneous Anisotropic Plates”, *Journal of Applied Mechanics*, Vol. 36, pp. 261-266, 1969.

18. Chaudhuri, R. A., “On Boundary-Discontinues Double Fourier Series Solution to a System of Completely Coupled P.D.E.’s”, *International Journal of Engineering Sciences,* Vol. 27, No. 9, pp. 1005-1022, 1989.

19. Chaudhuri, R. A., “On the Roles of Complementary and Admissible Boundary Constraints in Fourier Solutions to the Boundary Value Problems of Completely Coupled rth Order Pdes”, *Journal of Sound and Vibration*, Vol. 251, No. 2, pp. 261-313, 2002.

20. Green, A. E., “Double Fourier Series and Boundary Value Problems”, *Proceedings of Cambridge Philosophical Society*, Vol. 40, pp. 222-228, 1944.

21. Green, A. E. and R. F. S. Hearmon, “The Buckling of Flat Rectangular Plywood Plates”, *Philosophical Magazine*, Vol. 36, pp. 659-688, 1945.

22. Whitney, J. M., “Fourier Analysis of Clamped Anisotropic Plates”, *Journal of Applied Mechanics*, Vol. 38, pp. 530-532, 1971.

23. Whitney, J. M., “Analysis of Anisotropic Rectangular Plates”, *AIAA Journal,* Vol. 10, pp. 1544-1545, October 1972.

24. Whitney J. M. and A. W. Leissa, “Analysis of a Simply Supported Laminated Anisotropic Rectangular Plate”, *AIAA Journal*, Vol. 8, No. 1, pp. 28-33.

25. Chaudhuri, R. A., K. Balaraman and V. X. Kunukkasseril, “A Combined Theoretical and Experimental Investigation on Free Vibration of Thin Symmetrically Laminated Anisotropic Plates”, *Composite Structures*, Vol. 67, pp. 85-97, 2005.

26. Ali, M. M., A. Törn and S. Viitanen, "A Direct Search Variant of the Simulated Annealing Algorithm for Optimization Involving Continuous Variables", *Computers & Operations Research*, Vol. 29, pp. 87-102, 2002.

27. Jones, R. M., *Mechanics of Composite Materials,* 2nd ed., Taylor & Francis, 1999.

28. Cupial, P., "Calculation of the Natural Frequencies of Composite Plates by the Rayleigh-Ritz Method with Orthogonal Polynomials", *Journal of Sound and Vibration*, Vol. 201, No. 3, pp. 385-387, 1997.

29. Leissa, A. W. and Y. Narita, "Vibration Studies for Simply Supported Symmetrically Laminated Rectangular Plates", *Composite Structures*, Vol. 12, pp. 113-132, 1989.

30. Hobson, E. W., *The Theory of Functions of a Real Variable and the Theory of Fourier's Series,* Vol. 2, 2nd ed., Cambridge University Press, Cambridge, 1926.

REFERENCES NOT CITED

Abrate S., "Optimal Design of Laminated Plates and Shells", *Composite Structures*, Vol. 29, pp. 269-286, 1994.

Erdal, O., *Optimum Design of Composite Laminates Using Simulated Annealing*, M.S. Thesis, Boğaziçi University, 2004.

Fukunaga H., H. Sekine and M. Sato, "Optimal Design of Symmetric Laminated Plates for Fundamental Frequency", *Journal of Sound and Vibration*, Vol. 171, No. 2, pp. 219-229, 1994.

Glower, F. and A. K. Gary (editors), *Handbook of Metaheuristics*, Kluwer Academic Publishers, Boston, 2003.

Göker, G., *Vibration Analysis of Skew Fiber-Reinforced Composite Laminates Plates*, M.S. Thesis, Boğaziçi University, 1999.

Gürdal, Z., R. T. Haftka and P. Hajela, *Design and Optimization of Laminated Composite Materials*, John Wiley & Sons, New York, 1998.

Narita Y., "Maximum Frequency Design of Laminated Plates with Mixed Boundary Conditions", *International Journal of Solids and Structures*, Vol. 43, pp. 4342-4356, 2006.

Press, W. E., *Numerical Recipes in Pascal: The Art of Scientific Computing*, Cambridge University Press, Cambridge, 1989.

Reddy, J. N., *Mechanics of Laminated Composite Plates and Shells: Theory and Analysis*, CRC Press, Boca Raton, 2004.

Vinson, J. R. and R. L. Sierakowski, *Behavior of Structures Composed of Composite Materials*, 2nd ed., Kluwer Academic Publishers, Boston, 2002.